Original Article

Novel TNF-α Receptor 1 Antagonist Treatment Attenuates Arterial Inflammation and Intimal Hyperplasia in Mice

Manabu Kitagaki[1], Kikuo Isoda[2], Haruhiko Kamada[3], Takayuki Kobayashi[4], Shinichi Tsunoda[3], Yasuo Tsutsumi[3,5], Tomiharu Niida[2], Takehiko Kujiraoka[2], Norio Ishigami[2], Miya Ishihara[1], Osamu Matsubara[4], Fumitaka Ohsuzu[2] and Makoto Kikuchi[1]

[1]Medical Engineering, National Defense Medical College, Saitama, Japan
[2]Internal Medicine I, National Defense Medical College, Saitama, Japan
[3]Laboratory of Biopharmaceutical Research, National Institute of Biomedical Innovation, Osaka, Japan
[4]Basic Pathology, National Defense Medical College, Saitama, Japan
[5]Department of Toxicology and Safety Science, Graduate School of Pharmaceutical Sciences, Osaka University, Osaka, Japan

Aim: Tumor necrosis factor receptor 1 (TNFR1) participates importantly in arterial inflammation in genetically altered mice; however it remains undetermined whether a selective TNFR1 antagonist inhibits arterial inflammation and intimal hyperplasia. This study aimed to determine the effect and mechanism of a novel TNFR1 antagonist in the suppression of arterial inflammation.
Methods: We investigated intimal hyperplasia in IL-1 receptor antagonist-deficient mice two weeks after inducing femoral artery injury in an external vascular cuff model. All mice received intraperitoneal injections of TNFR1 antagonist (PEG-R1antTNF) or normal saline twice daily for 14 days.
Results: PEG-R1antTNF treatment yielded no adverse systemic effects, and we observed no significant differences in serum cholesterol or blood pressure in either group; however, selective PEG-R1antTNF treatment significantly reduced intimal hyperplasia (19,671±4,274 vs. 11,440±3,292 μm^2; $p=0.001$) and the intima/media ratio (1.86±0.43 vs. 1.34±0.36; $p=0.029$), compared with saline injection. Immunostaining revealed that PEG-R1antTNF inhibits Nuclear factor-κB (NF-κB), suppressing smooth muscle cell (SMC) proliferation and decreasing chemokine and adhesion molecule expression, and thus decreasing intimal hyperplasia and inflammation.
Conclusions: Our data suggest that PEG-R1antTNF suppresses SMC proliferation and inflammation by inhibiting NF-κB. This study highlights the potential therapeutic benefit of selective TNFR1 antagonist therapy in preventing intimal hyperplasia and arterial inflammation.

J Atheroscler Thromb, 2012; 19:36-46.

Key words; TNF receptor 1 antagonist, Cytokine, Inflammation, Intimal hyperplasia, Smooth muscle cell

Introduction

Tumor necrosis factor-α (TNF-α) possesses important proinflammatory properties that participate crucially in innate and adaptive immunity[1]. Due to its numerous effects on different cell types (e.g., macrophages, endothelial cells, and smooth muscle cells (SMCs)), TNF-α might contribute to arterial inflammation and intimal hyperplasia, including the induction of adhesion molecule expression of cell migration and proliferation[2,3].

TNF-α elicits responses through two receptors, TNF receptor 1 (TNFR1) and TNF-α receptor 2 (TNFR2). TNFR1 activates the majority of biological responses[4]. TNFR2 is mainly expressed in cells associated with the immune response, and TNFR2 signaling plays an important role in the biophylactic system[5]. Several previous studies have examined the effect of TNFR1 signaling on vascular physiology using TNFR1-deficient mice. Schreyer *et al.* demonstrated

Address for correspondence: Kikuo Isoda, Internal Medicine I, National Defense Medical College, 3-2, Namiki, Tokorozawa, Saitama, 359-8513, Japan
E-mail: isoda@ndmc.ac.jp
Received: April 18, 2011
Accepted for publication: August 9, 2011

an anti-atherogenic effect of TNFR1 signaling[6]. In another study, TNFR1 did not affect atherosclerosis in Apo E-deficient mice[7]. Conversely, Zhang *et al.* demonstrated that TNFR1 expression in the arterial wall contributed substantially to atherosclerosis in an arterial grafting model using TNFR1-deficient mice[8]. Furthermore, they demonstrated that TNF signaling via TNFR2 attenuated neointimal hyperplasia by reducing adhesion molecule expression and endothelial cell apoptosis in an arterial grafting model using TNFR2-deficient mice[9]. Xanthoulea *et al.* showed that atherosclerotic plaques are smaller in LDL receptor-deficient mice carrying TNFR1-deficient bone marrow compared to controls[10]. Taken together, these studies suggest that the role of TNF-α, TNFR1 and TNFR2 in vascular inflammation remains incompletely understood. As referred to above, several reports using genetically-altered mice suggested that TNFR1-specific blocking therapy may be the optimal therapy for arterial inflammation; however, no current data show that blocking with a TNFR1 antagonist contributes to the inhibition of arterial inflammation and atherogenesis. We therefore attempted to reveal the roles of these two TNF receptor subtypes in arterial inflammation *in vitro* and *in vivo* using a TNFR1 antagonist.

Recently, two types of TNF blocker, infliximab (chimeric TNF-α monoclonal antibody) and etanercept (soluble TNF receptor), have become available for the treatment of rheumatoid arthritis, and have proven to be efficacious. Previous reports showed that anti-TNF therapy improved endothelial function and decreased cardiovascular events associated with systemic inflammation of rheumatoid arthritis[11-13], but the therapy has its downsides. Inhibition of TNF-α function by anti-TNF therapy increases the chance of infection[14], whereas TNFR1-specific blocking therapy (inhibiting only TNFR1 signal, but not TNFR2 signal) has the potential to inhibit inflammation and offset the side effects of conventional TNF blockers.

More recently, our colleagues produced a novel TNFR1-selective antagonistic mutant TNF-α (R1antTNF) using phage display[15], and also developed PEGylated R1antTNF (PEG-R1antTNF), an agent that further enhances potential anti-inflammatory activity[16, 17]. The aim of the present study, therefore, was to clarify the effect of this novel TNFR1 antagonist on arterial inflammation and intimal hyperplasia.

Materials and Methods

Novel Tumor Necrosis Factor-α Receptor 1 Antagonist; R1antTNF and PEG-R1antTNF

Our colleagues developed R1antTNF and PEG-R1antTNF for use with a phage-display system. Briefly, they constructed a phage library that displays structural variants of human TNF, in which random amino acid sequences replace the 6 residues (amino acids 84-89) that are likely present in the TNF receptor-binding site from the crystal structure of the LT-α-TNFR1 complex. This phage library consisted of 1×10^7 independent recombinant clones. The phage selection that displays structural TNF variants (Panning) yielded the structural TNF variant R1antTNF with selectively high affinity for TNFR1 and inhibition of TNFR1 signaling. Compared with wild-type TNF-α, R1antTNF has superior affinity for TNFR1, but only one fifty-thousandth of affinity for TNFR2. PEG-R1antTNF is PEGylated R1antTNF, which PEG (polyethylene glycol; average molecular weigh 5,000) binds to N-terminal site of R1antTNF, thus improving circulatory retention[15-17].

To compare *in vivo* stability, we injected mice intraperitoneally with PEG-R1antTNF and R1antTNF, and measured serum levels at the indicated time points. In the R1antTNF group, serum concentration almost attained the limit of detection 12 h post-injection. In contrast, the retention time of PEG-R1antTNF in the circulation was considerably longer than R1antTNF[17].

Cell Culture

We purchased human umbilical vein endothelial cells (HUVECs) and human aortic smooth muscle cells (HASMCs) (Kurabo). After culturing HUVECs in HuMedia-EG2 and HASMCs in HuMedia-SG2 (Kurabo) with growth factor, fourth and seventh passage cells, respectively, were used for our experiment. HUVECs and HASMCs were cultured to confluence. After washing the dishes, HUVECs and HASMCs were cultured with 1 ng/mL human recombinant TNF-α (R&D systems) and 1 μg/mL R1antTNF for 5, 10, 30, 60 and 120min. The cells were lysed with Lysis Buffer (50 mM Tris-HCl, 150 mM NaCl, 1 mM EDTA, 1% TritonX-100, 50 mM NaF, 30 mM $Na_4O_7P_2$, 1 mM Na_3VO_4, protease inhibitor) and used for Western blotting.

SDS-PAGE and Western Blotting

Cell lysate and 2x protein sample buffer for SDS-PAGE (BIO-RAD) were mixed equally, and then 2-mercaptethanol was added at a final concentration

of 5%. After incubation at 100℃ for 10min, these samples were separated by 10-20% SDS-PAGE and transferred to a polyvinylidene difluoride (PVDF) membrane (Hoefer). The membrane was incubated with rabbit anti-phospho-nuclear factor-kappa B (pNF-κB) (Cell Signaling) diluted 1:1000, rabbit anti-phospho-endothelial/epithelial tyrosine kinase (pEtk) (Cell Signaling) diluted 1:1000 and mouse anti-human β-actin (BD Bioscience) diluted 1:30000 in 4% BlockAce (Dainippon Sumitomo Pharma), and then treated with goat anti-rabbit IgG-horseradish peroxidase (Cell Signaling) diluted 1:2000 and goat anti-mouse IgG-horseradish peroxidase (Sigma Aldrich) diluted 1:50000, respectively. Immunodetection was performed with chemiluminescent reagent; ECL-plus (GE Healthcare). The immunoblot was analyzed with an imaging system (LAS3000; Fuji Film), and bands density was estimated using Image J 1.14 (National Institutes of Health).

Reverse Transcription Quantitative PCR *in vitro*

We cultured HUVECs with 1 ng/mL human recombinant TNFα (R&D Systems) and 1 μg/mL R1antTNF for 24 hours. Total RNA from HUVECs was isolated with TRIzol (Invitrogen). Complimentary DNA was obtained using SuperScript Ⅲ Reverse Transcriptase (Invitrogen) according to the manufacturer's instructions. Quantitative mRNA expression was assessed by real-time PCR with Taqman PCR Master Mix (Applied Biosystems) using specific primers for ICAM-1 (Taqman gene expression assay; Applied Biosystems). Samples were run in duplicate on the 7900HT Fast Real-Time OCR system (Applied Biosystems).

Mice and Genotyping

Interleukin-1 receptor antagonist deficiency (IL-1Ra-/-) mice were generated in our laboratory by replacing the exons encoding the secreted form with the neo gene, as previously described[18]. IL-1Ra-/- mice showed excessive arterial inflammation and intimal hyperplasia after cuff injury[19].

Embryonic stem cells were aggregated with 2 (C57BL6J × DBA/2) F1 mice at the 8-cell stage. All 4 isoforms of IL-1Ra were destroyed and mutant mice were a background to C57BL/6J strain mice for 8 generations. To obtain homozygous mutant mice, heterozygous mice were intercrossed with each other. All studies were conducted according to the protocols approved by the National Defense Medical College Board for Studies in Experimental Animals.

Femoral Artery Injury and Treatment

To eliminate gender differences, we used only male mice. Eight-week-old mice were anesthetized by intraperitoneal injection of pentobarbital (50 mg/kg). We dissected the left femoral artery from its surrounding, as described previously[20]. Vascular injury was inflicted by placing a non-occlusive polyethylene cuff (length 2.0 mm; internal diameter 0.56 mm; Becton Dickinson) around the femoral artery. Mice received intraperitoneal injections of PEG-R1antTNF (experimental model; 3 μg twice daily) or normal saline (controls) twice daily for two weeks.

Plasma Lipid Measurement

A blood sample was collected from both groups at 14 days post-injury. Plasma total cholesterol, low-density lipoprotein (LDL) cholesterol, and high-density lipoprotein (HDL) cholesterol levels were measured by high performance liquid chromatography (HPLC) at Skylight Biotech Inc. (Akita, Japan) as described previously[21]. Plasma lipoproteins were analyzed by an on-line dual enzymatic method for simultaneous quantification of cholesterol according to the procedure described by Usui *et al.*[22].

Arterial Harvest and Morphometric Analysis

After measuring systolic blood pressure, the animals were euthanized by pentobarbital injection and the vascular tree perfused with 0.9% NaCl followed by 4% paraformaldehyde. Following perfusion, the femoral artery was harvested and fixed with 10% neutral-buffered formalin.

We embedded the artery in paraffin and cut 10 sections (each 5-μm thick) from 10 equally spaced locations. The slides were stained with hematoxylin-eosin and elastica van Gieson, and then examined and photographed using ECLIPS LV100 microscopy (Nikon). The luminal, neointimal, and medial areas were calculated using NIS element (Nikon). To determine the effect of PEG-R1antTNF on vascular remodeling, we defined the vessel area as the area inside external elastic lamina, and calculated the intima area/vessel area ratio.

Immunohistochemistry

Using anti-proliferating cell nuclear antigen (PCNA) antibody (1:100; Dako), α smooth muscle actin (SMA) antibody (Dako), and pNF-κB antibody (1:50; Santa Cruz Biotechnology, Santa Cruz), respectively, we conducted immunohistochemistry for proliferating, SMCs, and NF-κB activation on paraffin-embedded sections. Before immunostaining, sections were treated in a microwave oven in 0.1 mol/L citrate

buffer, pH 6.0. Endogenous peroxidase was blocked by incubation with 3% H_2O_2 in methanol for 5 min. Slides were incubated with normal swine serum (Vector Laboratories) for 10 minutes and then with primary antibody overnight at 4℃ at the concentrations described above. The sections were incubated with the complementary secondary antibody for 60 min. We visualized the sections using the Envison system (Dako) with DAB as the substrate. Conversely, we conducted immunohistochemistry on frozen sections of monocytes/macrophages, leukocyte adhesion molecules, and chemokines, using anti-CD11b antibody (1:50; BD Bioscience), anti-intracellular adhesion molecule 1 (ICAM-1) antibody (1:50 R&D Systems), and monocyte chemoattractant protein 1 (MCP-1) antibody (1:100; Santa Cruz Biotechnology), respectively. The secondary antibody was the biotinylated antibody (Dako). The sections were visualized with a Vectastain ABC kit (Vector Laboratories), using DAB as the substrate. The nuclei were counterstained with Mayer's hematoxylin solution. Negative control slides were incubated without a primary antibody.

Reverse Transcription Quantitative PCR

Total RNA from the liver, lung, thymus gland and femoral artery tissue was isolated with TRIzol (Invitrogen). Complimentary DNA was obtained using SuperScript Ⅲ Reverse Transcriptase (Invitrogen) according to the manufacturer's instructions. Quantitative mRNA expression was assessed by real-time PCR with Power SYBR Green PCR Master Mix (Applied Biosysytems) using primers specific for TNF-α (forward: TCC CAG GTT CTC TTC AAG GGA, reverse: GGT GAG GAG CAC GTA GTC GG), MCP-1 (forward: CCA CTC ACC TGC TAC TCA T, reverse: TGGTGA TCC TCTTGT AGC TCT CC) and GAPDH (forward: AAC TTT GGC ATT GTG GAA GG, reverse: ACA CAT TGG GGG TAG GAA CA). Samples were run in duplicate on the 7900HT Fast Real-Time PCR system (Applied Biosystems).

Statistical Analysis

Results are shown as the mean ± SD. Differences between groups were analyzed by Student's t test. $P<0.05$ was regarded as significant.

Results

R1antTNF Limited TNFα Induced NF-κB Activation in Endothelial Cells and Smooth Muscle Cells

Western blotting was used to examine pNF-κB expression in HUVECs and SMCs to ascertain whether R1antTNF inhibited TNFR1 signaling. pNF-κB peaked 30min after TNF-α stimulation and then deteriorated quickly. R1antTNF decreased pNF-κB expression in both HUVECs and SMCs compared with the control (**Fig. 1A**). Calculation of the pNF-κB/β-actin expression ratio 30 min after TNF-α stimulation showed that R1antTNF inhibition of pNF-κB expression was superior to the control in HUVECs (2.03 ± 0.57 vs. 1.30 ± 0.08: $p=0.045$) and SMCs (1.74 ± 0.16 vs. 1.17 ± 0.26: $p=0.009$) (**Fig. 1B**).

To determine the influence on TNFR2 signaling, we investigated the specific effect of phosphorylated pEtk on TNFR2 signaling. pEtk peaked 5 min after TNF-α stimulation in endothelial cells. We observed no significant differences in pEtk expression between groups (**Fig. 1C**).

Next, we evaluated mRNA levels of ICAM-1 in HUVECs using real-time PCR. Analysis revealed the reduction of mRNA levels of ICAM-1 in HUVECs with both TNF-α and R1antTNF compared with those with TNF-α only (2.11 ± 0.38 vs. 1.54 ± 0.23; $p=0.042$) (**Fig. 2**).

PEG-R1antTNF Treatment Yielded No Adverse in IL-1Ra-/- Mice

We investigated intimal hyperplasia in IL-1Ra-/- mice two weeks after femoral artery injury by an external vascular cuff model. Mice received intraperitoneal injections of PEG-R1antTNF (experimental model) or normal saline (controls) twice daily for two weeks. No adverse systemic effects of PEG-R1antTNF were observed and systolic blood pressure was similar between groups (**Table 1**). Moreover, plasma lipid analysis revealed no statistically significant differences in total cholesterol, LDL cholesterol, and HDL cholesterol between these groups (**Table 2**).

To examine how R1antTNF influences the whole body, we evaluated TNF-α mRNA expression levels in the liver, lung, and thymus gland two weeks after administration using reverse transcription quantitative PCR. We observed a tendency toward inhibited TNF-α mRNA expression in the liver of the PEG-R1antTNF group, but the difference was not statistically significant compared with controls (1.98 ± 1.41 vs. 0.66 ± 0.33: $p=0.075$). Expression levels of TNF-α mRNA in the lung and thymus gland of the PEG-R1antTNF group did not differ significantly from the controls (**Table 3**).

PEG-R1antTNF Inhibited Intimal Hyperplasia in IL-1Ra-/- Arteries Post-Injury

We investigated the effect of PEG-R1antTNF treatment on the femoral arteries of IL-1Ra-/- mice following cuff-induced injury. **Fig. 3** shows representa-

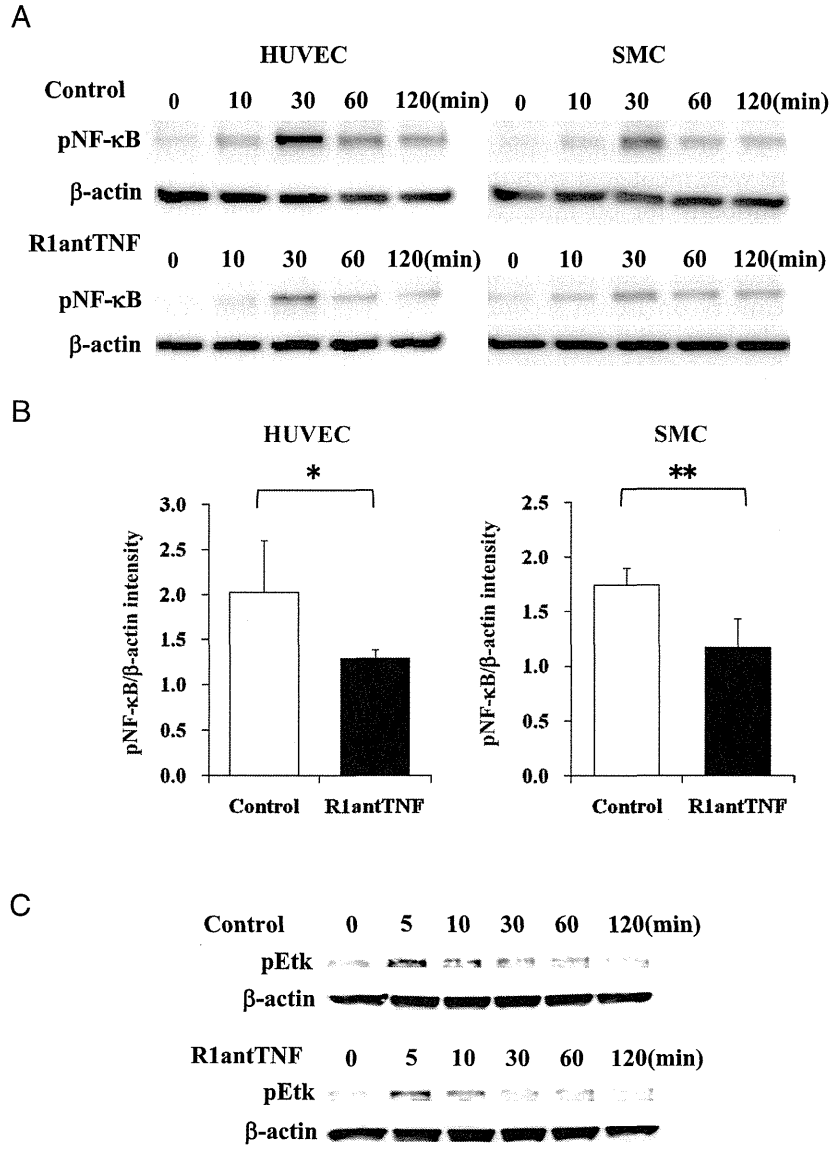

Fig. 1. R1antTNF significantly inhibited the expression of pNF-κB in HUVECs and SMCs.

(A) Expression levels of pNF-κB peaked 30 min after stimulation in Western blot analysis. (B) Bar graphs show band density 30 min after stimulation in control and R1antTNF treatment. Data are expressed as the mean ± SD ($n=4$). *$p<0.05$, **$p<0.01$. (C) There was no difference in the expression levels of pEtk between R1antTNF and the control group in Western blot analysis.

tive cross sections of femoral arteries harvested 14 days post-injury. Immunostaining for α-SMA showed that intimal hyperplasia consisted of SMCs. PEG-R1antTNF but not saline treatment inhibited intimal hyperplasia (**Fig. 3A**). Morphometric analysis revealed significantly decreased intimal hyperplasia in mice receiving PEG-R1antTNF treatment compared with controls (19,671 ± 4,274 vs. 11,440 ± 3,292 μm^2; $p=0.001$) (**Fig. 3B**). PEG-R1antTNF treatment also decreased the intima/media ratio (1.86 ± 0.43 vs. 1.34 ± 0.36; $p=0.029$) and the intima/vessel area ratio (0.35 ± 0.06 vs. 0.21 ± 0.11; $p=0.011$) compared with saline controls (**Fig. 3C** and **D**); therefore, our results suggest that PEG-R1antTNF significantly decreases intimal hyperplasia.

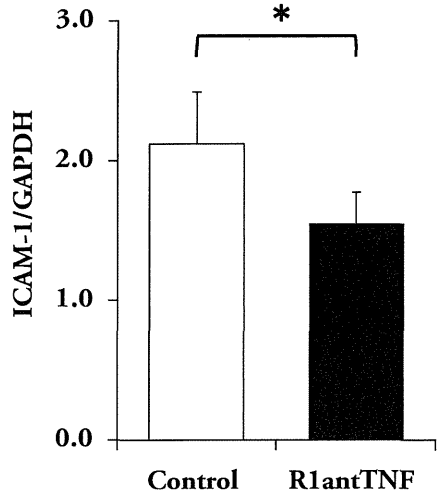

Fig. 2. R1antTNF inhibited the expression of ICAM-1 mRNA in HUVECs after TNF-α stimulation. mRNA levels of ICAM-1 were assessed with real-time PCR. Data are expressed as the mean ± SD ($n=4$). *$p<0.05$.

Inhibition of NF-κB Activation by PEG-R1antTNF Decreased Expression of Chemokine and Adhesion Molecule

To examine TNF-α and MCP-1 expression in the injured artery 5 days post-surgery, real-time PCR was performed to evaluate mRNA levels of TNF-α and MCP-1. Mice receiving PEG-R1antTNF treatment showed inhibited expression of TNF-α (2.62 ± 1.47 vs. 1.06 ± 0.74; $p=0.029$) and MCP-1 (1.34 ± 0.77 vs. 0.50 ± 0.24; $p=0.048$) mRNA compared with control mice (**Fig. 4A**).

To determine the effect of PEG-R1antTNF on injured arteries, immunostaining for pNF-κB was performed at 7 and 14 days post-injury. Fewer pNF-κB- positive nuclei were observed in the intima of PEG-R1antTNF-treated mice at 7 and 14 days than in controls (**Fig. 4B**). ICAM-1 and MCP-1 expressions were also investigated, and both increased in endothelial cells from controls but not PEG-R1antTNF-treated mice (**Fig. 4C**). Immunostaining also revealed fewer macrophages in the intima of PEG-R1antTNF-treated mice than in controls (**Fig. 4C**).

To determine cell proliferating activity, immunostaining for PCNA was performed 14 days post-injury. PEG-R1antTNF decreased the number of PCNA-positive nuclei compared with controls. Furthermore, the expression of PCNA-positive nuclei considerably accorded with α-SMA-positive cells (**Fig. 5A**). Quantitative analysis also revealed that PEG-R1antTNF-treated mice had fewer PCNA-positive nuclei than controls 14 days post-injury (**Fig. 5B**). These data suggest that PEG-R1antTNF exerts a vascular anti- inflammatory effect by inhibiting NF-κB.

Table 1. Measurement of blood pressure and heart rate at 14 days post-injured

	Control	R1antTNF	*p* value
Blood pressure (mmHg)	106.6 ± 10.0	110.6 ± 5.3	0.451
Heart rate (bpm)	654.2 ± 48.6	666.6 ± 56.9	0.721

Results are expressed as the mean ± SD

Table 2. Plasma lipid analysis at 14 days post-injured

	Control	R1antTNF	*p* value
Total Cholesterol (mg/dL)	73.11 ± 8.30	68.87 ± 8.37	0.399
LDL Cholesterol (mg/dL)	21.69 ± 4.47	18.37 ± 2.33	0.137
HDL Cholesterol (mg/dL)	46.73 ± 6.75	44.79 ± 9.02	0.683

Results are expressed as the mean ± SD

Table 3. TNF-α mRNA expression at 14 days post-injured

	Control	R1antTNF	*p* value
Liver	1.98 ± 1.41	0.66 ± 0.33	0.075
Lung	1.10 ± 0.18	1.10 ± 0.74	0.994
Thymus Gland	0.98 ± 0.53	1.09 ± 0.32	0.728

Value is TNF-α mRNA/GAPDH mRNA ratio. Results are expressed as the mean ± SD

Discussion

We demonstrate here for the first time that a specific TNFR1 antagonist inhibited intimal hyperplasia following arterial inflammation induced by cuff injury in IL-1Ra-/- mice with excessive post-injury inflammation. Previous reports demonstrated that TNFR1 participates in exacerbated intimal hyperplasia in wire-injured artery[23] or arteriovenous grafts[8] using the mouse carotid artery. Moreover, a study using double-deficient (TNFR1 and LDL receptor) mice showed decreasing sizes of atherosclerotic plaque[24]. Thus, TNF-α plays an important role, and TNF signaling through TNFR1 participates significantly in the development of intimal hyperplasia and atherosclerosis; however, these findings were observed in genetically altered mice, and the current literature does not show how the TNFR1 antagonist might affect arterial inflammation.

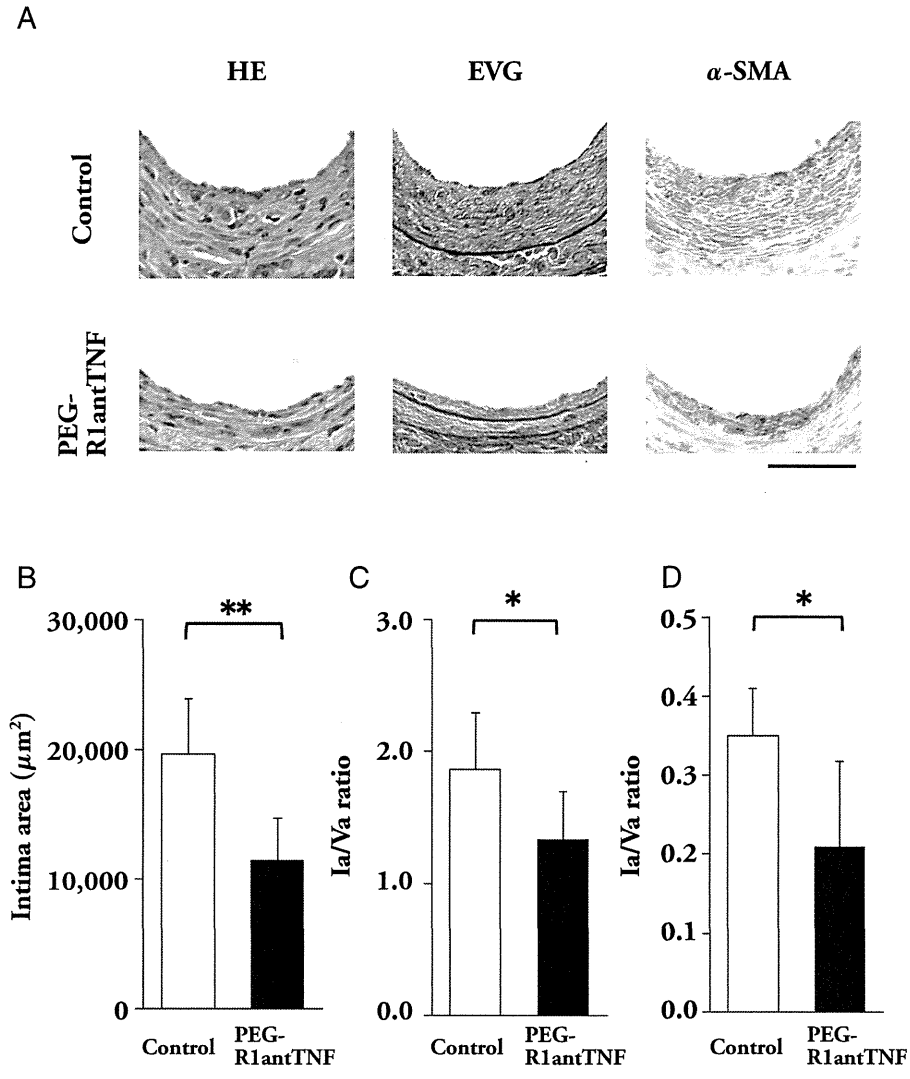

Fig. 3. PEG-R1antTNF significantly inhibited intimal hyperplasia in IL-1 Ra−/− arteries post-injury.

(A) Microscopic appearance of hematoxylin and eosin staining (left), elastica van Gieson staining (middle) and α-SMA staining (right) of femoral artery from control (upper panels) and PEG-R1antTNF (lower panels) groups 14 days post-injury. Scale bar = 50 μm. Bar graphs show intimal area (B), intima/media area ratio (C), and intima/vessel area ratio (D). Data are expressed as the mean ± SD (n = 7 for each). $^{*}p < 0.05$, $^{**}p < 0.01$.

The present study investigated the relationship between TNF signaling and arterial inflammation, revealing for the first time that TNFR1 signaling blocked by a TNFR1 antagonist might affect arterial inflammation and intimal hyperplasia in cuff-injured IL-1Ra-/- mice with severe inflammation around the artery, similar to Takayasu's disease[25]. Initially, we used wild-type C57BL/6J mice for the cuff injury model, but treatment induced little neointima formation in the control group. The lack of significant differences in intima area (3,222.9 ± 1,640.3 vs. 2,383.9 ± 618.7 μm^2; $p = 0.267$) and the intima area/media area ratio (0.278 ± 0.119 vs. 0.201 ± 0.060; $p = 0.179$) between the control and R1antTNF treatment group made it difficult to examine whether R1antTNF suppresses arterial inflammation and intimal hyperplasia. Previously, we reported that deficiency of IL-1Ra promotes intimal hyperplasia after femoral artery injury[18, 26]. We further determined that TNF-α deficiency suppresses aortitis in IL-1Ra-/- mice[27]. Thus,

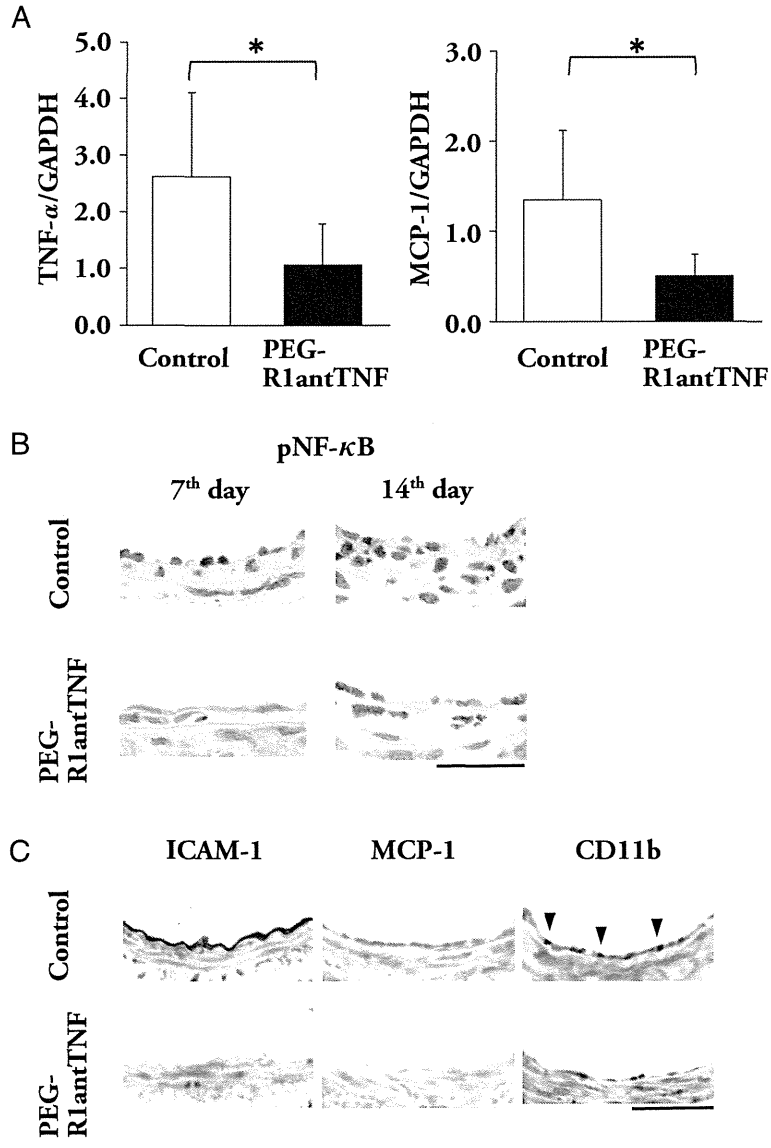

Fig. 4. PEG-R1antTNF suppressed TNF-α, adhesion molecule and chemokine, and activation of NF-κB.

(A) These graphs showed the amount of TNF-α (left; $n=7$) and MCP-1 (right; $n=5$) mRNA expression 5 days post-injury. Data are expressed as the mean ± SD. $^*p<0.05$. The result of immunostaining for pNF-κB-positive nucleus 7 and 14 days post-injury (B), expression of ICAM-1 (C; left), MCP-1 (C; middle), and CD11b (C; right) 7 days post-injury. Scale bar = 50 μm.

our findings suggest that TNF-α participates importantly in the development of arterial inflammation in IL-1Ra-/- mice. Consequently, we used IL-1Ra-/- mice in the present study because we believe that these mice were suitable for evaluating the effect of TNFR1 blocking therapy in active arterial inflammation induced by cuff injury.

The dose of PEG-R1antTNF in our study was determined according to a previous report showing PEG-R1antTNF was effective for the suppression of collagen-induced arthritis in mice[17]. The PEG-R1antTNF dose was not changed based on body weight, as infliximab and etanercept are also injected at the same dose independently of the body weight of the patients. Taken together, we think that the dose of PEG-R1ant TNF must be relevant in our study.

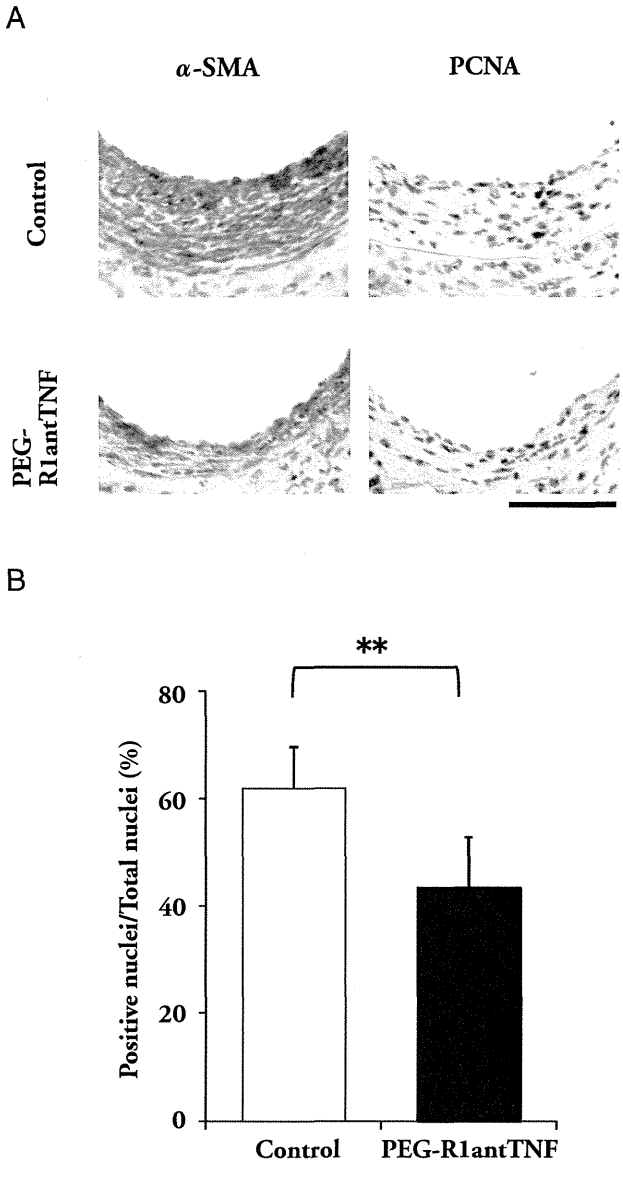

Fig. 5. PEG-R1antTNF inhibited cell proliferation in injured arteries.

(A) Representative photographs of α-SMA and PCNA staining of injured arteries 14 days post-injury. Scale bar=50 μm. (B) Bar graph shows the number of PCNA-positive nuclei in the intima. Data are expressed as the mean ± SD ($n=6$). $^{**}p<0.01$.

A previous report showed that TNF-α activates IKK, induces the phosphorylation and ubiquitination of IκB, and activates NF-κB[28]. NF-κB is activated mainly via TNFR1 signaling, but only poorly via TNFR2-TNF receptor-associated factor 2 signaling[29]. NF-κB regulates macrophage migration and the expression of adhesion factor (ICAM-1)[30] and chemokine (MCP-1). NF-κB also regulates both the proliferation and migration of vascular SMCs[31-34]. Our results showed that blocking TNFR1 with R1antTNF decreased macrophage accumulation as well as ICAM-1 and MCP-1 expression by inhibiting NF-κB activation in endothelial cells and SMCs in the injured artery. Thus, TNFR1 signaling participates importantly in the development of intimal hyperplasia following arterial inflammation. Additionally, we show a relationship among inhibited intimal hyperplasia, suppressed NF-κB activation, adhesion factor and chemokine expression.

Zhang *et al.* examined the effect of TNF signaling through TNFR2 for intimal hyperplasia, demonstrating that TNFR2 signaling inhibits neointimal formation by decreasing adhered cells and endothelial cells apoptosis. They also showed that Etk/Bmx, a non-receptor tyrosine kinase, contributed to these results[9]. A previous study observed the anti-apoptotic effect of TNFR2, which specifically activates Etk/Bmx. TNFR2 also induces the activation, proliferation and migration of endothelial cells. Another study suggested that Etk/Bmx participates importantly in angiogenesis induced by TNF-α[35]. Thus, TNFR1-specific blocking therapy might aid the earlier regeneration of endothelial cells and inhibit intimal hyperplasia compared with TNF blocking therapy, which blocks both TNFR1 and TNFR2 signaling. Therefore, we examined whether R1antTNF treatment altered pEtk/Bmx expression in endothelial cells. Our results revealed no significant difference in pEtk/Bmx expression between groups. Similarly, our colleague, who used an index of GM-CSF production by TNF-α in PC60-R2 cells (a mouse-rat fusion hybridoma consisting of human TNFR2-transfected PC60 cells)[15], reported that R1antTNF did not affect bioactivity via TNFR2. These data suggest that R1antTNF does not stimulate endothelial cell regeneration in *in vitro* studies. In the future, we will examine whether R1antTNF treatment exerts an effect on Etk/Bmx activation via TNFR2 *in vivo*.

TNF-α forms a trimeric structure with various bioactivities[36]. We found that R1antTNF reacted with endogenous TNF-α to form a heterotrimer *in vitro* (unpublished data), possibly affecting the half-life and bioactivity of endogenous TNF-α *in vivo*. Thus, it remains undetermined whether the *in vivo* effects of R1antTNF might result only from inhibited TNFR1 signaling. Determining whether the trimer formation of R1antTNF and endogenous TNF-α might change the effect will require further study.

TNF blocking therapy improves vascular endothelial dysfunction and reduces cardiovascular events associated with inflammation in patients with rheu-

matoid arthritis[12, 13]; however, there has been much concern over the reactivation of viral infection caused by TNF blockade[14]. Shibata *et al.* compared the effects of PEG-R1antTNF and etanercept on antiviral immunity using a recombinant adenovirus vector and showed that PEG-R1antTNF did not reactivate viral infection, unlike etanercept[17]. Their results indicated that use of PEG-R1antTNF may reduce side effects such as increased susceptibility to viral infection due to its TNFR1 selectivity. Additionally, transmembrane TNF (tmTNF), the prime activating ligand of TNFR2[5], was reported to be sufficient to control Mycobacterium tuberculosis infection[37, 38], indicating the importance of TNF/TNFR2 function in this bacterial infection. Because PEG-R1antTNF does not bind TNFR2, PEG-R1antTNF cannot inhibit the interaction of tmTNF with TNFR2; therefore, we believe that PEG-R1antTNF would also have reduced side effects in the context of bacterial infection.

In conclusion, the present study shows that a selective TNFR1 antagonist, PEG-R1antTNF, suppresses arterial inflammation by inhibiting NF-κB activation and chemokine expression. Thus, inhibited TNFR1 signaling may provide a new therapeutic target for preventing intimal hyperplasia and inflammation.

Acknowledgements

We thank Mr. Shigehiro Kitada and Ms. Kozue Suzuki (Division of Basic Pathology, National Defense Medical College) for pathological support. We also thank the staff of the Institute of Laboratory Animals, National Defense Medical College for animal care.

Notice of Grant Support

This research was supported in part by National Defense Medical College Grant for Young Scientist (M.K.) and National Defense Medical College grant H14 (K.I.) and H18 (K.I.)

Disclosure

None.

References

1) Popa C, Netea MG, van Riel PL, van der Meer JW, Stalenhoef AF: The role of TNF-alpha in chronic inflammatory conditions, intermediary metabolism, and cardiovascular risk. J Lipid Res, 2007; 48: 751-762
2) Wajant H, Pfizenmaier K, Scheurich P: Tumor necrosis factor signaling. Cell Death Differ, 2003; 10: 45-65
3) Fan J, Watanabe T: Inflammatory reactions in the pathogenesis of atherosclerosis. J Atheroscler Thromb, 2003; 10: 63-71
4) Kleemann R, Zadelaar S, Kooistra T: Cytokines and atherosclerosis: a comprehensive review of studies in mice. Cardiovasc Res, 2008; 79: 360-376
5) Grell M, Douni E, Wajant H, Löhden M, Clauss M, Maxeiner B, Georgopoulos S, Lesslauer W, Kollias G, Pfizenmaier K, Scheurich P: The transmembrane form of tumor necrosis factor is the prime activating ligand of the 80 kDa tumor necrosis factor receptor. Cell, 1995; 83: 793-802
6) Schreyer SA, Peschon JJ, LeBoeuf RC: Accelerated atherosclerosis in mice lacking tumor necrosis factor receptor p55. J Biol Chem, 1996; 271: 26174-26178
7) Blessing E, Bea F, Kuo CC, Campbell LA, Chesebro B, Rosenfeld ME: Lesion progression and plaque composition are not altered in older apoE-/- mice lacking tumor necrosis factor-alpha receptor p55. Atherosclerosis, 2004; 176: 227-232
8) Zhang L, Peppel K, Sivashanmugam P, Orman ES, Brian L, Exum ST, Freedman NJ: Expression of tumor necrosis factor receptor-1 in arterial wall cells promotes atherosclerosis. Arterioscler Thromb Vasc Biol, 2007; 27: 1087-1094
9) Zhang L, Sivashanmugam P, Wu JH, Brian L, Exum ST, Freedman NJ, Peppel K: Tumor necrosis factor receptor-2 signaling attenuates vein graft neointima formation by promoting endothelial recovery. Arterioscler Thromb Vasc Biol, 2008; 28: 284-289
10) Xanthoulea S, Gijbels MJ, van der Made I, Mujcic H, Thelen M, Vergouwe MN, Ambagts MH, Hofker MH, de Winther MP: P55 tumour necrosis factor receptor in bone marrow-derived cells promotes atherosclerosis development in low-density lipoprotein receptor knock-out mice. Cardiovasc Res, 2008; 80: 309-318
11) Szekanecz Z, Kerekes G, Soltész P: Vascular effects of biologic agents in RA and spondyloarthropathies. Nat Rev Rheumatol, 2009; 5: 677-684
12) Hürlimann D, Forster A, Noll G, Enseleit F, Chenevard R, Distler O, Béchir M, Spieker LE, Neidhart M, Michel BA, Gay RE, Lüscher TF, Gay S, Ruschitzka F: Anti-tumor necrosis factor-alpha treatment improves endothelial function in patients with rheumatoid arthritis. Circulation, 2002; 106: 2184-2187
13) Jacobsson LT, Turesson C, Gülfe A, Kapetanovic MC, Petersson IF, Saxne T, Geborek P: Treatment with tumor necrosis factor blockers is associated with a lower incidence of first cardiovascular events in patients with rheumatoid arthritis. J Rheumatol, 2005; 32: 1213-1218
14) Bongartz T, Sutton AJ, Sweeting MJ, Buchan I, Matteson EL, Montori V: Anti-TNF antibody therapy in rheumatoid arthritis and the risk of serious infections and malignancies: systematic review and meta-analysis of rare harmful effects in randomized controlled trials. JAMA, 2006; 295: 2275-2285
15) Shibata H, Yoshioka Y, Ohkawa A, Minowa K, Mukai Y, Abe Y, Taniai M, Nomura T, Kayamuro H, Nabeshi H, Sugita T, Imai S, Nagano K, Yoshikawa T, Fujita T, Nakagawa S, Yamamoto A, Ohta T, Hayakawa T, Mayumi T,

Vandenabeele P, Aggarwal BB, Nakamura T, Yamagata Y, Tsunoda S, Kamada H, Tsutsumi Y: Creation and X-ray structure analysis of the tumor necrosis factor receptor-1-selective mutant of a tumor necrosis factor-alpha antagonist. J Biol Chem, 2008; 283: 998-1007
16) Yamamoto Y, Tsutsumi Y, Yoshioka Y, Nishibata T, Kobayashi K, Okamoto T, Mukai Y, Shimizu T, Nakagawa S, Nagata S, Mayumi T: Site-specific PEGylation of a lysine- deficient TNF-alpha with full bioactivity. Nat Biotechnol, 2003; 21: 546-552
17) Shibata H, Yoshioka Y, Abe Y, Ohkawa A, Nomura T, Minowa K, Mukai Y, Nakagawa S, Taniai M, Ohta T, Kamada H, Tsunoda S, Tsutsumi Y: The treatment of established murine collagen-induced arthritis with a TNFR1-selective antagonistic mutant TNF. Biomaterials, 2009; 30: 6638-6647
18) Horai R, Asano M, Sudo K, Kanuka H, Suzuki M, Nishihara M, Takahashi M, Iwakura Y: Production of mice deficient in genes for interleukin (IL)-1alpha, IL-1beta, IL-1alpha/beta, and IL-1 receptor antagonist shows that IL-1beta is crucial in turpentine -induced fever development and glucocorticoid secretion. J Exp Med, 1998; 187: 1463-1475
19) Isoda K, Shiigai M, Ishigami N, Matsuki T, Horai R, Nishikawa K, Kusuhara M, Nishida Y, Iwakura Y, Ohsuzu F: Deficiency of interleukin-1 receptor antagonist promotes neointimal formation after injury. Circulation, 2003; 108: 516-518
20) Isoda K, Nishikawa K, Kamezawa Y, Yoshida M, Kusuhara M, Moroi M, Tada N, Ohsuzu F: Osteopontin plays an important role in the development of medial thickening and neointimal formation. Circ Res, 2002; 91: 77-82
21) Isoda K, Sawada S, Ayaori M, Matsuki T, Horai R, Kagata Y, Miyazaki K, Kusuhara M, Okazaki M, Matsubara O, Iwakura Y, Ohsuzu F: Deficiency of interleukin-1 receptor antagonist deteriorates fatty liver and cholesterol metabolism in hypercholesterolemic mice. J Biol Chem, 2005; 280: 7002-7009
22) Usui S, Hara Y, Hosaki S, Okazaki M: A new on-line dual enzymatic method for simultaneous quantification of cholesterol and triglycerides in lipoproteins by HPLC. J Lipid Res, 2002; 43: 805-814
23) Zimmerman MA, Reznikov LL, Sorensen AC, Selzman CH: Relative contribution of the TNF-alpha receptors to murine intimal hyperplasia. Am J Physiol Regul Integr Comp Physiol, 2003; 284: R1213-1218
24) Xanthoulea S, Thelen M, Pöttgens C, Gijbels MJ, Lutgens E, de Winther MP: Absence of p55 TNF receptor reduces atherosclerosis, but has no major effect on angiotensin II induced aneurysms in LDL receptor deficient mice. PLoS One, 2009; 4: e6113
25) Johnston SL, Lock RJ, Gompels MM: Takayasu arteritis: a review. J Clin Pathol, 2002; 55: 481-486
26) Isoda K, Ohsuzu F: The effect of interleukin-1 receptor antagonist on arteries and cholesterol metabolism. J Atheroscler Thromb, 2006; 13: 21-30
27) Matsuki T, Isoda K, Horai R, Nakajima A, Aizawa Y, Suzuki K, Ohsuzu F, Iwakura Y: Involvement of tumor necrosis factor-alpha in the development of T cell-dependent aortitis in interleukin-1 receptor antagonist-deficient mice. Circulation, 2005; 112: 1323-1331
28) Chen G, Goeddel DV: TNF-R1 signaling: a beautiful pathway. Science, 2002; 296: 1634-1635
29) McFarlane SM, Pashmi G, Connell MC, Littlejohn AF, Tucker SJ, Vandenabeele P, MacEwan DJ. Differential activation of nuclear factor-kappaB by tumour necrosis factor receptor subtypes. TNFR1 predominates whereas TNFR2 activates transcription poorly. FEBS Lett, 2002; 515: 119-126
30) Mackay F, Loetscher H, Stueber D, Gehr G, Lesslauer W: Tumor necrosis factor alpha (TNF-alpha)-induced cell adhesion to human endothelial cells is under dominant control of one TNF receptor type, TNF-R55. J Exp Med, 1993; 177: 1277-1286
31) Ip JH, Fuster V, Badimon L, Badimon J, Taubman MB, Chesebro JH: Syndromes of accelerated atherosclerosis: role of vascular injury and smooth muscle cell proliferation. J Am Coll Cardiol, 1990; 15: 1667-1687
32) Ross R: Atherosclerosis--an inflammatory disease. N Engl J Med, 1999; 340: 115-126
33) Zhou Z, Connell MC, MacEwan DJ: TNFR1-induced NF-kappaB, but not ERK, p38MAPK or JNK activation, mediates TNF-induced ICAM-1 and VCAM-1 expression on endothelial cells. Cell Signal, 2007; 19: 1238-1248
34) Collins T, Cybulsky MI: NF-kappa B: pivotal mediator or innocent bystander in atherogenesis? J Clin Invest, 2001; 107: 255-264
35) Pan S, An P, Zhang R, He X, Yin G, Min W: Etk/Bmx as a tumor necrosis factor receptor type 2-specific kinase: role in endothelial cell migration and angiogenesis. Mol Cell Biol, 2002; 22: 7512-7523
36) Smith RA, Baglioni C: The active form of tumor necrosis factor is a trimer. J Biol Chem, 1987; 262: 6951-6954
37) Olleros ML, Guler R, Corazza N, Vesin D, Eugster HP, Marchal G, et al: Transmembrane TNF induces an efficient cell-mediated immunity and resistance to Mycobacterium bovis bacillus Calmette-Guerin infection in the absence of secreted TNF and lymphotoxin-alpha. J Immunol, 2002; 168: 3394-3401
38) Saunders BM, Tran S, Ruuls S, Sedgwick JD, Briscoe H, Britton WJ: Transmembrane TNF is sufficient to initiate cell migration and granuloma formation and provide acute, but not long-term, control of Mycobacterium tuberculosis infection. J Immunol, 2005; 174: 4852-4859

Laboratory of Biopharmaceutical Research[1], National Institute of Biomedical Innovation; Laboratory of Toxicology and Safety Science[2], Graduate School of Pharmaceutical Sciences; The Center for Advanced Medical Engineering and Informatics[3]; Laboratory of Biomedical Innovation[4], Graduate School of Pharmaceutical Sciences, Osaka University, Osaka, Japan

Rho GDP-dissociation inhibitor alpha is associated with cancer metastasis in colon and prostate cancer

T. YAMASHITA[1,2,*], T. OKAMURA[1,*], K. NAGANO[1,*], S. IMAI[1], Y. ABE[1], H. NABESHI[1,2], T. YOSHIKAWA[1,2], Y. YOSHIOKA[1,2,3], H. KAMADA[1,3], Y. TSUTSUMI[1,2,3], S. TSUNODA[1,3,4]

Received July 7, 2011, accepted August 5, 2011

Shin-ichi Tsunoda, Ph.D, Laboratory of Biopharmaceutical Research, National Institute of Biomedical Innovation, 7-6-8 Saito-Asagi, Ibaraki, Osaka 567-0085, Japan.
tsunoda@nibio.go.jp
**These authors contributed equally to the work.*

Pharmazie 67: 253–255 (2012) *doi: 10.1691/ph.2012.1630*

Since metastasis is one of the most important prognostic factors in colorectal cancer, development of new methods to diagnose and prevent metastasis is highly desirable. However, the molecular mechanisms leading to the metastatic phenotype have not been well elucidated. In this study, a proteomics-based search was carried out for metastasis-related proteins in colorectal cancer by analyzing the differential expression of proteins in primary versus metastasis focus-derived colorectal tumor cells. Protein expression profiles were determined using a tissue microarray (TMA), and the results identified Rho GDP-dissociation inhibitor alpha (Rho GDI) as a metastasis-related protein in colon and prostate cancer patients. Consequently, Rho GDI may be useful as a diagnostic biomarker and/or a therapeutic to prevent colon and prostate cancer metastasis.

1. Introduction

Colorectal cancer is known as a major metastatic cancer, and 40–50% of patients already have a metastatic focus at presentation. Moreover, the 5-year survival of these patients is under 10% (Davies et al. 2005). Thus, metastasis is one of the most important prognostic factors in colorectal cancer. In order to improve rates of cancer remission, it will be necessary to clarify the detailed molecular mechanisms of cancer metastasis and to utilize this information to establish new diagnostic and therapeutic techniques. Many researchers have searched for metastasis-related molecules (Liu et al. 2010; Shuehara et al. 2011) using proteomics techniques (Hanash 2003). Comprehensive mapping of the molecular changes during metastasis would greatly improve our understanding of the recurrence and management of cancer. However, the knowledge gained so far in these studies has not been sufficient to improve cancer remission rates.

Here we show the potential of Rho GDI as a metastasis-related protein in colon and prostate cancer patients. In order to identify metastasis-related proteins, the protein expression patterns of human colorectal cancer cells with different metastatic characters were compared. Because these cells were derived from the same patient (SW480: a surgical specimen of a primary colon adenocarcinoma, SW620: a lymph node metastatic focus), cancer metastasis-related protein candidates could be effectively sought without background variations due to differences between individuals. Furthermore, by analyzing the expression of candidate proteins in many clinical samples using a TMA, we attempted to validate the association of these candidates with metastasis. TMA is a slide glass containing many clinical tissues, and it enables one to carry out a high-throughput analysis by evaluating the relationship between expression profiles of each candidate molecule and clinical information such as metastasis. (Imai et al. 2011; Yoshida et al. 2011).

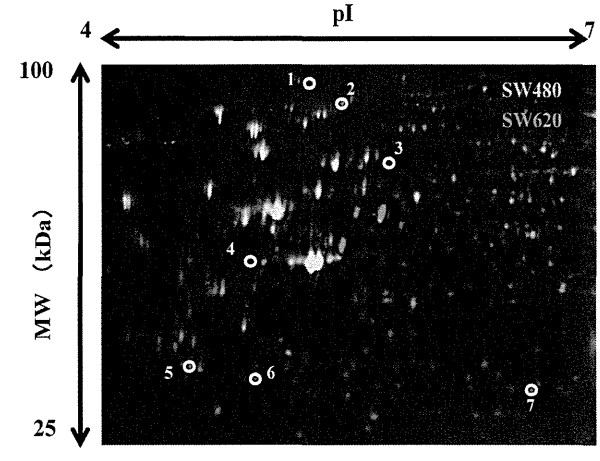

Fig. 1: 2D-DIGE image of fluorescently-labeled proteins from different metastatic human colorectal cancer cells. SW480 is human colorectal cancer cell line derived from a primary tumor and SW620 is derived from a metastatic focus from the same patient. Proteins from the colon cancer cells (SW480, SW620) were labeled with Cy3 and Cy5 respectively, and analyzed by 2D electrophoresis. The differentially-expressed spots (white circles) were then identified by LC-UHR TOF/MS

Table 1: High expression proteins in SW620 compared to SW480

	Accession	Protein name	MW (kDa)	pI	Ratio (SW620 / SW480)
1	P12109	collagen alpha-1(VI) chain	108.6	5.3	1.53
2	Q15459	splicing factor 3A subunit 1	88.9	5.2	1.61
3	P13797	T-plastin	70.9	5.5	1.59
4	P60709	actin cytoplasmic 1	42.1	5.3	1.50
5	P63104	14-3-3 zeta/delta	27.9	4.7	1.63
6	P52565	Rho GDP-dissociation inhibitor 1 (Rho GDI)	23.3	5.0	1.90
7	P30041	Peroxiredoxin-6 (PRDX6)	25.1	6.0	1.86

2. Investigations, results and discussion

In order to search for metastasis-related proteins, we analyzed differentially-expressed proteins between SW480 and SW620 by two-dimensional differential in-gel electrophoresis (2D-DIGE) (Fig. 1). As a result, 7 spots with at least a 1.5-fold-altered expression level were found by quantitative analysis, and these spots were identified by mass spectrometry (Table 1). Three molecules having a high SW620/SW480 expression ratio indicating a strong association with cancer metastasis were identified: Rho GDP-dissociation inhibitor alpha (Rho GDI), peroxiredoxin-6 (PRDX6) and 14-3-3 zeta/delta.

The expression profiles of these proteins were analyzed by immunohistochemistry using the TMA with colon cancer and multiple cancer tissues. Results of this analysis indicated that expression of PRDX6 and 14–3-3 zeta/delta had no relationship to the clinical status of cancer metastasis (data not shown). On the other hand, in positive cases of lymph node metastasis, the expression ratio of Rho GDI was significantly higher than in the negative cases. Furthermore, the same trend was seen when tissues from prostate cancer patients were analyzed (Table 2).

To confirm these results, the expression levels of Rho GDI protein in colon cancer cell lines with different metastatic potential (SW480 < SW620 < SW620-OK1 < SW620-OK2: Characteristics of SW620-OK1 and SW620-OK2 are described in *Experimental*) were investigated by western blot analysis (Fig. 2). The expression of Rho GDI was found to be up-regulated with the development of metastatic characteristics. These results suggested that Rho GDI is correlated with cancer metastasis.

Rho GDI has been identified as key regulator of Rho family GTPases. Activation of growth factor receptors and integrins can promote the exchange of GDP for GTP on Rho proteins (Bishop et al. 2000). Furthermore, GTP-bound Rho proteins interact with a range of effector molecules to modulate their activity or localization, and this leads to changes in cell behavior. It is clear that Rho family GTPases are involved in the control of cell morphology and motility (Etienne-Manneville et al. 2002; Hall et al. 1997; Van Aelst et al. 1997). The importance of Rho protein and Rho GDI in cancer progression, particularly in the area of metastasis, is becoming increasingly evident. Recently, some reports have indicated that the expression of Rho GDI was correlated with colorectal and breast cancer metastasis (Zhao et al. 2008; Kang et al. 2010). Thus, our findings are consistent with these reports and further suggest that the expression of Rho GDI is also correlated with prostate cancer metastasis. Consequently, Rho GDI should be considered as a diagnostic marker or new therapeutic target for cancer metastasis.

3. Experimental

3.1. Cell lines

SW480 is a human colorectal cancer cell line derived from a primary focus and SW620 is derived from a metastatic focus of the same patient. These cells were purchased from American Type Culture Collection and maintained at 37 °C using Leibovitz's L-15 medium (Wako) supplemented with 10% FCS. SW620-OK1 and -OK2 were established by the following procedure: 1×10^6 SW620 cells were injected into the spleens of nu/nu mice. After 8 weeks, SW620-OK1 was established from a liver metastatic focus. Furthermore, SW620-OK2 was established from SW620-OK1 using the same procedures.

3.2. 2D-DIGE analysis

Cell lysates were prepared from SW480 and SW620 and then solubilized with 7 M urea, 2 M thiourea, 4% CHAPS and 10 mM Tris-HCl (pH 8.5). The lysates were labeled at the ratio of 50 μg proteins: 400 pmol Cy3 or Cy5 protein-labeling dye (GE Healthcare Biosciences) in dimethylformamide according to the manufacturer's protocol. Briefly, the labelled samples were mixed with rehydration buffer (7 M urea, 2 M thiourea, 4% CHAPS, 2% DTT, 2% Pharmalyte (GE Healthcare Biosciences)) and applied to a 24-cm immobilized pH gradient gel strip (IPG-strip pH 4–7 NL) for separation in the first dimension. Samples for the spot-picking gel were prepared without labelling by Cy-dyes. For the second dimension separation, the IPG-strips were applied to SDS-PAGE gels (10% polyacrylamide and 2.7% N,N'-diallyltartardiamide gels). After electrophoresis, the gels were scanned with a laser fluoroimager (Typhoon Trio, GE Healthcare Biosciences). The spot-picking gel was scanned after staining with Deep Purple Total Protein Stain (GE Healthcare Biosciences). Quantitative analysis of protein spots was carried out with Decyder-DIA software (GE Healthcare Biosciences). For the antigen spots of interest, spots of 1 mm × 1 mm in size were picked using Ettan Spot Picker (GE Healthcare Biosciences).

3.3. In-gel tryptic digestion

Picked gel pieces were digested with trypsin as described below. The gel pieces were destained with 50% acetonitrile/50 mM NH_4HCO_3 for 20 min twice, dehydrated with 75% acetonitrile for 20 min, and then dried using a centrifugal concentrator. Next, 5 μl of 20 μl/ml trypsin (Promega) solution was added to each gel piece and incubated for 16 h at 37 °C. Three solutions were used to extract the resulting peptide mixtures from the gel pieces. First, 50 μl of 50% (v/v) acetonitrile in 0.1% (v/v) formic acid (FA) was added to the gel pieces, which were then sonicated for 5 min. Next, we collected the solution and added 80% (v/v) acetonitrile in 0.1% FA. Finally, 100% acetonitrile was added for the last extraction. The peptides were dried and then re-suspended in 10 μl of 0.1% FA.

3.4. Mass spectrometry and database search

Extracted peptides were analyzed by liquid chromatography Ultra High Resolution time-of-flight mass spectrometry (LC-UHR TOF/MS; maXis, Bruker Daltonics). The Mascot search engine (http://www.matrixscience.com) was initially used to query the entire theoretical tryptic peptide database as well as SwissProt (http://www.expasy.org/, a public domain database pro-

Table 2: Expression profile of Rho GDI in primary cancers with or without lymph node metastasis

	Number of Rho GDI positive cases (positive ratio)	
	in metastasis negative cases	in metastasis positive cases
Colon cancer*	11/14 (79%)	19/19 (100%)
Prostate cancer*	18/23 (78%)	11/11 (100%)

* $p < 0.05$: Mann Whitney U test

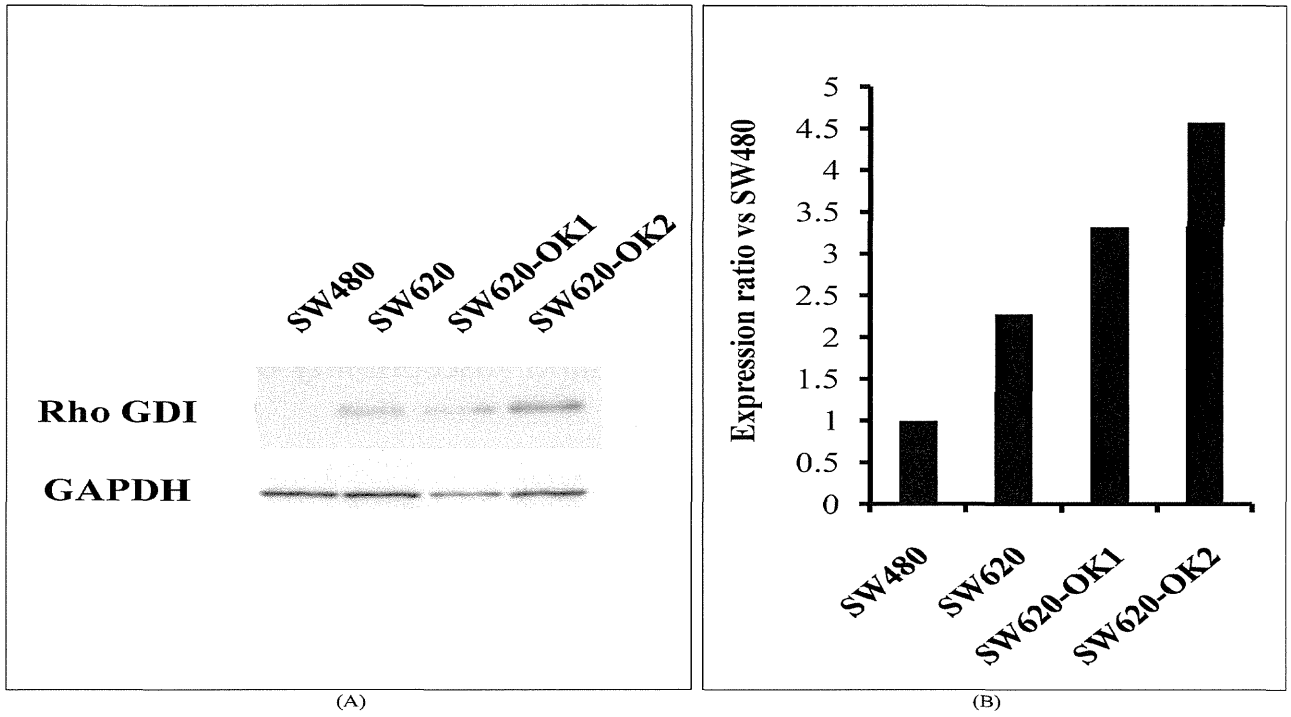

Fig. 2: Rho GDI expression levels in colon cancer cell lines with different metastatic abilities. Rho GDI expression levels in colon cancer cell lines (SW480, SW620, SW620-OK1, SW620-OK2) analyzed by western blotting (A). SW620-OK1, SW620-OK2 have been established as high metastatic sub-lines of SW620 using a mouse metastasis model. Intensity of the western blotting images was quantified by densitometry (B)

vided by the Swiss Institute of Bioinformatics). The search query assumed the following: (i) the peptides were monoisotopic (ii) methionine residues may be oxidized (iii) all cysteines are modified with iodoacetamide.

3.5. TMA Immunochemical staining

TMA slides with human colon cancer samples or multiple cancer samples (Biomax) were de-paraffinated in xylene and rehydrated in a graded series of ethanol washes. Heat-induced epitope retrieval was performed while maintaining the Target Retrieval Solution pH 9 (Dako) at the desired temperature according to manufacturer's instructions. After the treatment, endogenous peroxidase was blocked with 0.3% H_2O_2 in Tris-buffer saline (TBS) for 5 min. After washing twice with TBS, TMA slides were incubated with 10% BSA blocking solution for 30 min. The slides were then incubated with the anti-Rho GDI (Santa Cruz Biotechnology) for 60 min. After washing three times with wash buffer (Dako), each series of sections was incubated for 30 min with Envision + Dual Link (Dako). The reaction products were rinsed twice with wash buffer and then developed in liquid 3, 3'-diaminobenzidine (Dako) for 3 min. After the development, sections were counterstained with Mayer's hematoxylin. All procedures were performed using AutoStainer (Dako).

3.6. TMA Immunohistochemistry scoring

The optimized staining conditions for TMAs corresponding to human colon as well as multiple cancers were determined based on the co-existence of both positive and negative cells in the same tissue sample. Signals were considered positive when reaction products were localized in the expected cellular component. The criteria for scoring of stained tissues were as follows: the distribution score was 0 (0%), 1 (1–50%) or 2 (51–100%), indicating the percentage of positive cells among all tumor cells present in one tissue. The intensity of the signal (intensity score) was scored as 0 (no signal), 1 (weak), 2 (moderate) or 3 (marked). The distribution and intensity scores were then summed into a total score (TS) of TS0 (sum = 0), TS1 (sum = 2), TS2 (sum = 3), and TS3 (sum = 4–5). Throughout this study, TS0 or TS1 was regarded as negative, whereas TS2 or TS3 were regarded as positive.

3.7. Western Blot

Expression of Rho GDI in colon cancer cells was detected by anti-Rho GDI (Santa Cruz Biotechnology) and HRP conjugated anti-mouse IgG antibody (Sigma) using the ECL-plus system. Equal amounts of protein loading were confirmed by parallel β-actin immunoblotting, and signal quantification was performed by densitometric scanning.

Acknowledgements: This study was supported in part by Grants-in-Aid for Scientific Research from the Ministry of Education, Culture, Sports, Science and Technology of Japan, and from the Japan Society for the Promotion of Science (JSPS). This study was also supported in part by Health Labor Sciences Research Grants from the Ministry of Health, Labor and Welfare of Japan.

References

Bishop AL, Hall A (2000) Rho GTPases and their effector proteins. Biochem J 348: 241–255.

Davies RJ, Miller R, Coleman N (2005) Colorectal cancer screening: prospects for molecular stool analysis. Nat Rev Cancer 5: 199–209.

Etienne-Manneville S, Hall A (2002) Rho GTPases in cell biology. Nature 420: 629–635.

Hall A (1997). Rho GTPases and the Actin cytoskeleton. Science 279: 509–514.

Hanash S (2003) Disease proteomics. Nature 422: 226–232.

Imai S, Nagano K, Yoshida Y, Okamura T, Yamashita T, Abe Y, Yoshikawa T, Yoshioka Y, Kamada H, Mukai Y, Nakagawa S, Tsutsumi Y, Tsunoda S (2011). Development of an antibody proteomics system using a phage antibody library for efficient screening of biomarker proteins. Biomaterials 32: 162–169.

Kang S, Kim MJ, An H, Kim BG, Choi YP, Kang KS, Gao MQ, Park H, Na HJ, Kim HK, Yun HR, Kim DS, Cho NH (2010) Proteomic molecular portrait of interface zone in breast cancer. J Proteome Res 9: 5638–5645.

Liu R, Wang K, Yuan K, Wei Y, Huang C (2010) Integrative oncoproteomics strategies for anticancer drug discovery. Expert Rev Proteomics 7: 411–429.

Sahai E (2007). Illuminating the metastatic process. Nat Rev Cancer 7: 737–749.

Suehara Y, Tochigi N, Kubota D, Kikuta K, Nakayama R, Seki K, Yoshida A, Ichikawa H, Hasegawa T, Kaneko K, Chuman H, Beppu Y, Kawai A, Kondo T (2011) Secernin-1 as a novel prognostic biomarker candidate of synovial sarcoma revealed by proteomics. J Proteomics 74: 829–842.

Van Aelst L, D'Souza-Schorey C (1997) Rho GTPases and signaling networks. Genes Dev 11: 2295–2322.

Yoshida Y, Yamashita T, Nagano K, Imai S, Nabeshi H, Yoshikawa T, Yoshioka Y, Abe Y, Kamada H, Tsutsumi Y, Tsunoda S (2011) Limited expression of reticulocalbin-1 in lymphatic endothelial cells in lung tumor but not in normal lung. Biochem Biophys Res Commun 405: 610–614.

Zhao L, Wang H, Li J, Liu Y, Ding Y (2008) Overexpression of Rho GDP-dissociation inhibitor alpha is associated with tumor progression and poor prognosis of colorectal cancer. J Proteome Res 7: 3994–4003.

Biochemical and Biophysical Research Communications 421 (2012) 140–144

Contents lists available at SciVerse ScienceDirect

Biochemical and Biophysical Research Communications

journal homepage: www.elsevier.com/locate/ybbrc

Annexin A4 is a possible biomarker for cisplatin susceptibility of malignant mesothelioma cells

Takuya Yamashita [a,b,1], Kazuya Nagano [a,1], So-ichiro Kanasaki [a,b], Yuka Maeda [a,b], Takeshi Furuya [a,b], Masaki Inoue [a], Hiromi Nabeshi [b], Tomoaki Yoshikawa [a,b], Yasuo Yoshioka [a,b,c], Norio Itoh [b], Yasuhiro Abe [a], Haruhiko Kamada [a,c], Yasuo Tsutsumi [a,b,c], Shin-ichi Tsunoda [a,c,d,*]

[a] Laboratory of Biopharmaceutical Research, National Institute of Biomedical Innovation, 7-6-8 Saito-Asagi, Ibaraki, Osaka 567-0085, Japan
[b] Laboratory of Toxicology and Safety Science, Graduate School of Pharmaceutical Sciences, Osaka University, 1-6 Yamadaoka, Suita, Osaka 565-0871, Japan
[c] The Center for Advanced Medical Engineering and Informatics, Osaka University, 1-6 Yamadaoka, Suita, Osaka 565-0871, Japan
[d] Laboratory of Biomedical Innovation, Graduate School of Pharmaceutical Sciences, Osaka University, 1-6 Yamadaoka, Suita, Osaka 565-0871, Japan

ARTICLE INFO

Article history:
Received 27 March 2012
Available online 4 April 2012

Keywords:
Malignant mesothelioma
Cisplatin susceptibility
Annexin A4
Biomarker
Proteomics

ABSTRACT

Mesothelioma is a highly malignant tumor with a poor prognosis and limited treatment options. Although cisplatin (CDDP) is an effective anticancer drug, its response rate is only 20%. Therefore, discovery of biomarkers is desirable to distinguish the CDDP-susceptible versus resistant cases. To this end, differential proteome analysis was performed to distinguish between mesothelioma cells of different CDDP susceptibilities, and this revealed that expression of annexin A4 (ANXA4) protein was higher in CDDP-resistant cells than in CDDP-susceptible cells. Furthermore, ANXA4 expression levels were higher in human clinical malignant mesothelioma tissues than in benign mesothelioma and normal mesothelial tissues. Finally, increased susceptibility was observed following gene knockdown of ANXA4 in mesothelioma cells, whereas the opposite effect was observed following transfection of an ANXA4 plasmid. These results suggest that ANXA4 has a regulatory function related to the cisplatin susceptibility of mesothelioma cells and that it could be a biomarker for CDDP susceptibility in pathological diagnoses.

1. Introduction

Malignant mesothelioma is an aggressive neoplasm located on serosal membrane surfaces such as the pleura, and less frequently the peritoneum, and it has a poor outcome. The five-year survival rate is only about 5%. On the other hand, it is well known that asbestos is the major causative agent in the development of this disease [1–3]. Moreover, malignant mesothelioma takes 40–50 years to develop following exposure to asbestos. Because of its adiabatic potential, asbestos was commonly used as a building material in the 1960–1970s. Thus, an increase in mesothelioma patients is expected in the future. Patients with pleural malignant mesothelioma commonly present with an effusion associated with breathlessness that is often accompanied by chest-wall pain and a cough. After confirming the diagnosis, many patients are treated by intensive multidirectional approaches that combine cytoreductive surgery with intrapleural or intraperitoneal chemotherapy [4–8]. However, cytoreductive surgery is not always possible for patients with extensive intraperitoneal disease. Thus, the role of chemotherapy in malignant mesothelioma is critically important.

CDDP is an extensively used anticancer drug for the treatment of malignant mesothelioma, although the response rate is only about 20% [9–12]. A major problem with CDDP treatment of malignant mesothelioma patients is the development of CDDP insusceptibility. Thus, there is an urgent need to further our understanding of the pathogenesis of malignant mesothelioma, particularly with respect to the expression of proteins that confer drug susceptibility, in order to develop novel therapeutic strategies. In this study, a proteomic analysis was performed using high- and low-CDDP-susceptible malignant mesothelioma cells to identify candidate proteins associated with CDDP susceptibility.

2. Materials and methods

2.1. Cells

H28, H2052, H2452, H226 and MSTO-221H were purchased from American Type Culture Collection and maintained in RPMI1640 medium (Wako) containing 10% fetal calf serum (Biowest). Human mesothelial cells (HMC) were purchased from

* Corresponding author at: Laboratory of Biopharmaceutical Research, National Institute of Biomedical Innovation, 7-6-8 Saito-Asagi, Ibaraki, Osaka 567-0085, Japan. Fax: +81 72 641 9817.
E-mail address: tsunoda@nibio.go.jp (S.-i. Tsunoda).
[1] These authors contributed equally to this work.

0006-291X/$ - see front matter © 2012 Elsevier Inc. All rights reserved.
http://dx.doi.org/10.1016/j.bbrc.2012.03.144

Sciencell and cultured in Mesothelial Cell Growth Medium (ZenBio) under a 5% CO_2 atmosphere at 37 °C.

2.2. Measurement of cisplatin susceptibility in malignant mesothelioma cells

Malignant mesothelioma cells were seeded into 96-well microplates and cultured overnight. Various concentrations of CDDP were added to each well, the plates were incubated for 24 h, and cell viability was measured using Cell count reagent SF (Nacalai tesque). Absorbance was measured using a microplate reader (Bio-Rad) at test and reference wavelengths of 450 and 650 nm, respectively.

2.3. Proteomic analysis using two dimensional differential in-gel electrophoresis

For proteomic analysis, quantitative analysis was performed using two dimensional differential in-gel electrophoresis (2D-DIGE). Cell lysates were prepared from H28 and H2052 and then solubilized with 7 M urea, 2 M thiourea, 4% CHAPS and 10 mM Tris–HCl (pH 8.5). The lysates were labeled at the ratio of 50 μg proteins: 400 pmol Cy3 or Cy5 protein-labeling dye (GE Healthcare Biosciences) in dimethylformamide according to the manufacturer's protocol. The labelled samples were mixed with rehydration buffer (7 M urea, 2 M thiourea, 4% CHAPS, 2% DTT, 2% Pharmalyte (GE Healthcare Biosciences)) and applied to a 24-cm immobilized pH gradient gel strip (IPG-strip pH 4–7) for separation in the first dimension. For the second dimension separation, the IPG-strips were treated with iodoacetamide and applied to SDS–PAGE gels (10% polyacrylamide and 2.7% *N,N′*-diallyltartardiamide gels). After electrophoresis, the gels were scanned with a laser fluoroimager (Typhoon Trio, GE Healthcare Biosciences). The spot-picking gel was scanned after staining with Deep purple total protein stain (GE Healthcare Biosciences). Quantitative analysis of protein spots was carried out with Decyder-DIA software (GE Healthcare Biosciences). For the antigen spots of interest, spots of 1 mm × 1 mm in size were picked using Ettan Spot Picker (GE Healthcare Biosciences).

2.4. In-gel tryptic digestion

Picked gel pieces were destained with 50% acetonitrile/50 mM NH_4HCO_3 for 20 min twice, dehydrated with 75% acetonitrile for 20 min, and then dried using a centrifugal concentrator. Five microliter of 20 μg/ml trypsin (Promega) solution was added to each gel piece and the pieces were incubated for 16 h at 37 °C. The digested peptides were extracted sequentially using 50%, 80%, and 100% acetonitrile and then dried before being suspended in 10 μl of 0.1% formic acid.

2.5. Mass spectrometry and database search

Extracted peptides were analyzed by liquid chromatography ultra high resolution time-of-flight mass spectrometry (LC-UHR TOF-MS/MS; maXis, Bruker Daltonics). The Mascot search engine (http://www.matrixscience.com) was initially used to query the entire theoretical tryptic peptide database as well as SwissProt (http://www.expasy.org/, a public domain database provided by the Swiss Institute of Bioinformatics). The search query assumed the following: (i) the peptides were mono-, di- or tri-isotopic, (ii) methionine residues may be oxidized, (iii) all cysteines were modified with carbamidomethyl.

2.6. Western blot

The cell lysates were separated in 10% SDS–polyacrylamide gels and transferred to Immobilon membranes (Millipore). After blocking by 4% block ace (DS Pharma Biomedical) for 1 h at room temperature, the blots were reacted with primary antibodies in a buffer containing 0.4% block ace, and then with the appropriate peroxidase-conjugated secondary antibodies in the same buffer. Expression of ANXA4 in malignant mesothelioma cells was detected by mouse anti-human ANXA4 (Abnova: 1D3) followed by an HRP-conjugated anti-mouse IgG antibody (Sigma–Aldrich) using the ECL-plus system (GE Healthcare Biosciences). Equal amounts of protein loading were confirmed by parallel β-actin immunoblotting, and signal quantification was performed by densitometric scanning.

2.7. Immunohistochemistry staining

Human mesothelioma and normal tissue sections were deparaffinated in xylene and rehydrated in a graded series of ethanol dilutions. Heat-induced epitope retrieval was performed by incubating at different temperatures following the manufacturer's instructions using Target Retrieval Solution pH 9 (Dako). After heat-induced epitope retrieval treatment, endogenous peroxidase was blocked with a peroxidase blocking reagent (Dako). Following peroxidase blocking, the slides were incubated with 10% bovine serum albumin (BSA) solution for 30 min at room temperature. The slides were then incubated for 60 min with anti-human ANXA4 monoclonal antibody (9 μg/ml) in 3% BSA at room temperature. After washing 3 times with wash buffer (Dako), the slides were incubated for 30 min with ENVISION + Dual Link (Dako) at room temperature. They were then washed final 3 times and stained with 3,3′-diaminobenzidine. After development, the slides were lightly counterstained with Mayer's hematoxylin and mounted with resinous mounting medium.

2.8. Cisplatin susceptibility in cells transfected with ANXA4-siRNA and ANXA4-plasmid

H28 was transfected with ANXA4-siRNA (target sequence: AAGGATATCACAGAAGGATAT, Qiagen) using Hyperfect reagent (Qiagen) according to the manufacturer's instructions. In contrast, H2052 was transfected with ANXA4-pcDNA 3.1 (a gift from Naka T: Laboratory for Immune Signal, National Institute of Biomedical Innovation) using FuGENE HD transfection reagent (Roche). After transfection, the cells were treated with various concentrations of CDDP for 36 h (ANXA4-siRNA) or 24 h (ANXA4-pcDNA 3.1). Cell viability was measured as described above.

2.9. Statistical analysis

Differences in tumor volumes between the control and target groups were compared using the unpaired Student's *t*-test.

3. Results

3.1. CDDP susceptibility in malignant mesothelioma cells

Cell viability following CDDP treatment was examined to determine which cell lines had higher or lower susceptibility to CDDP. Among five tested mesothelioma cell lines, H2052 was the most and H28 the least susceptible cell line (Fig. 1). The IC_{50} values of H28, H2052, H2452, H226 and MSTO-221H were 154.5, 27.8, 66.0, 87.5 and 49.5 μM, respectively.

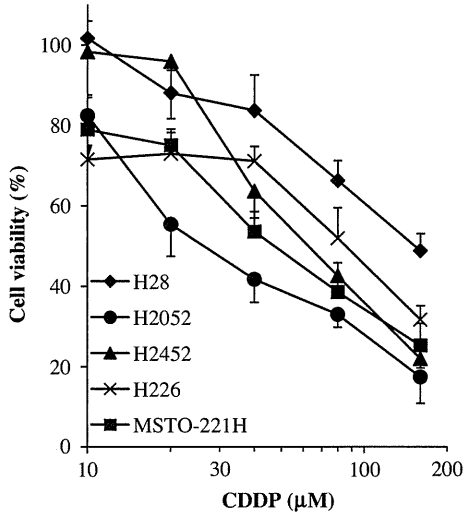

Fig. 1. Susceptibility of malignant mesothelioma cells to CDDP. Mesothelioma cells, H28, H2052, H2452, H226 and MSTO-221H were cultured with various concentrations of CDDP for 24 h 37 °C under 5% CO_2. Cell viability was assayed using the WST-8 assay. Maximal cell viability (100%) was obtained by incubating cells without CDDP. Data are shown as means and standard deviations ($n = 4$).

3.2. Identification of differentially expressed proteins by 2D-DIGE and MS

In order to search for CDDP susceptibility-related proteins, differential proteome analysis between H2052 and H28 cell lines was performed to search for CDDP susceptibility-related proteins (Fig. 2). Quantitative image analysis indicated that a total of eight protein spots representing > 2.0-fold alteration in expression were found and then identified by MS analysis (Table 1). Among those eight proteins, we focused on ANXA4 because this protein plays an important role in membrane stability. Previous reports have indicated that ANXA4 is associated with chemoresistance against platinum-based anticancer drugs in human lung, colon [13] and ovarian cancer [14].

3.3. ANXA4 expression analysis in human malignant mesothelioma cells and mesothelial tissues

Correlations between the expression levels in five malignant mesothelioma cell lines with CDDP-susceptibility were examined using western blot analysis to validate the identified proteins as CDDP susceptibility-related proteins. ANXA4 was expressed at a higher level in H28 cells relative to the other four CDDP-susceptible malignant mesothelioma cell lines (Fig. 3A and B). Expression of ANXA4 in human mesothelial tissue was analyzed by immunohistochemistry staining with an anti-human ANXA4 monoclonal antibody. Fig. 3C indicates that ANXA4 was expressed at higher levels in human malignant mesothelioma tissues than in benign mesothelioma tissues and normal mesothelial tissues.

3.4. Gene regulation of ANXA4 in malignant mesothelioma cells by knockdown and overexpression

ANXA4-siRNA and ANXA4-pcDNA 3.1 were next transfected to H28 and H2052 before CDDP treatment to evaluate correlations between ANXA4 expression levels and CDDP susceptibility. The IC_{50} values of [H28/non treat: H28/control-siRNA: H28/ANXA4-siRNA] were [80.0 μM: 71.8 μM: 15.5 μM] and [H2052/control-pcDNA 3.1: [H2052/ANXA4-pcDNA 3.1] were [55.2 μM: 89.7 μM], respectively (Fig. 4A–D). These results suggested that the CDDP susceptibility of H28 cells was increased by ANXA4-siRNA transfection and that of H2052 cells was decreased by ANXA4-pcDNA 3.1 transfection.

4. Discussion

In this study, a proteomic analysis was performed based on 2D-DIGE using malignant mesothelioma cell lines to identify candidate proteins associated with CDDP susceptibility (Figs. 1 and 2). Eight proteins that were differentially expressed in H28 cells compared with H2052 cells were identified (Table 1). ANXA4 was found to be expressed at a higher level in H28 cells relative to levels in CDDP-susceptible malignant mesothelioma cells by western blot

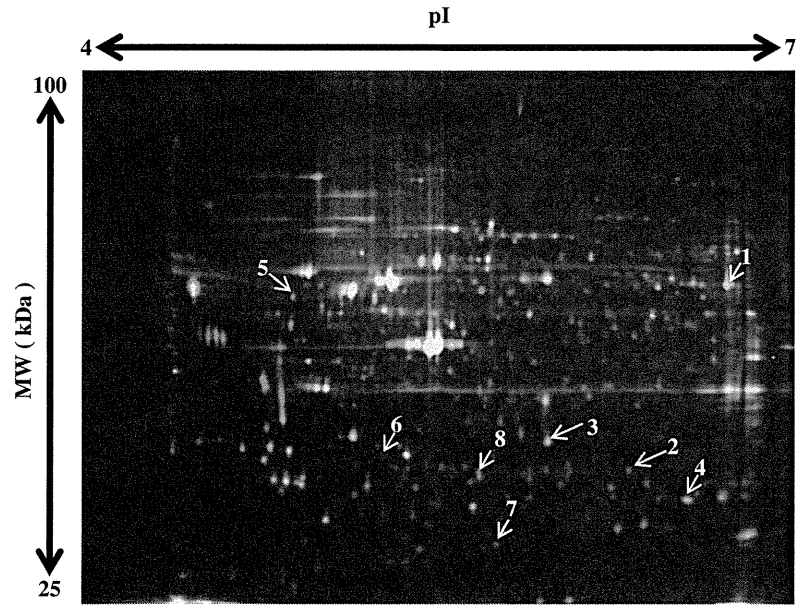

Fig. 2. 2D-DIGE image of fluorescently labeled proteins from human mesothelioma cell lines H28 and H2052. Proteins from high- and low-susceptible mesothelioma cells (H2052, H28) were labeled with cy3 and cy5, respectively, and 2D electrophoresis was performed. The differentially expressed spots in H28 indicated by white arrows were then identified by LC-TOF-MS/MS. Table 1 contains additional information about the identified proteins.

Table 1
Proteins expressed at higher or lower levels in H28 compared to H2052.

No.	Accession number	Protein name	pI	MW (kDa)	Expression ratio (H28/H2052)
1	P11413	Glucose-6-phosphate 1-dehydrogenase	6.4	59.3	21.0
2	P78417	Glutathione *S*-transferase omega-1	6.2	27.6	7.4
3	P09525	Annexin A4	5.6	35.9	3.6
4	P30041	Peroxiredoxin-6	6.0	25.0	3.5
5	Q09028	Histone-binding protein RBBP4	4.7	47.7	3.0
6	P07195	L-lactate dehydrogenase B chain	5.7	36.6	2.9
7	P32119	Peroxiredoxin-2	5.7	21.9	0.03
8	Q9Y696	Chloride intracellular channel protein 4	5.5	28.8	0.13

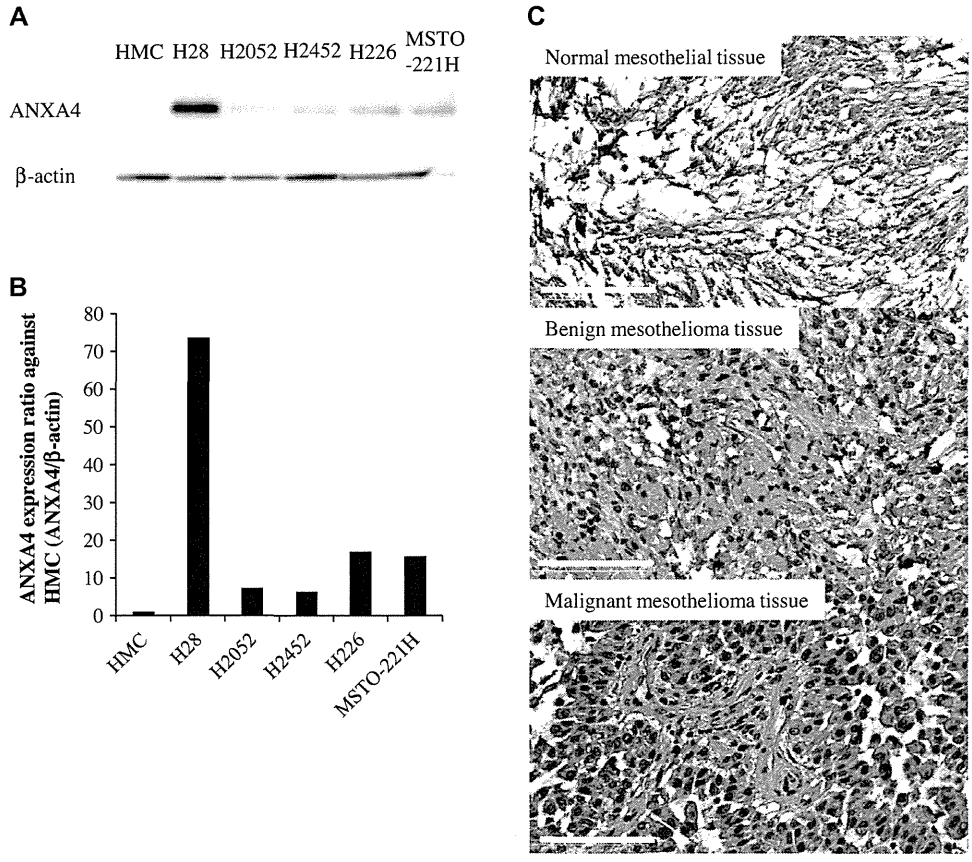

Fig. 3. ANXA4 expression analysis in human malignant mesothelioma cells and mesothelial tissues. ANXA4 expression levels in human primary mesothelial cells, HMC, and mesothelioma cell lines (H28, H2052, H2452, H226, MSTO-221H) were analyzed by western blotting (A). Intensity of the western blotting images was quantified by densitometry (B). Expression of ANXA4 in human mesothelial tissues was analyzed by immunostaining using an anti-human ANXA4 antibody (C). Top, middle and bottom panels are normal mesothelial, benign and malignant mesothelioma tissues, respectively. The tissue sections were counterstained using hematoxylin. Representative 400 × photomicrographs presented (bar: 100 μm).

analysis (Fig. 3A and B). Furthermore, ANXA4 was expressed in malignant mesothelioma tissue but not in benign mesothelial tumor and normal mesothelial tissues (Fig. 3C). Thus, ANXA4 was expressed in CDDP-susceptible malignant mesothelioma cells and specifically in malignant mesothelioma tissues. These results indicate that ANXA4 expression in malignant mesothelioma cells may be correlated with CDDP susceptibility, although this relationship must be validated in future studies of human clinical malignant mesothelial cases. The CDDP susceptibility of H28 cells was actually increased by ANXA4 knockdown, and that of H2052 cells was decreased by ANXA4 overexpression (Fig. 4). Thus, these results suggest that ANXA4 plays an important role in chemoresistance against CDDP.

ANXA4 has already been characterized as a regulator of cell membranes with calcium dependency [15–17]. Recently, some studies have reported the protein is associated with membrane permeability [18], ion channels [19] and exocytosis [20,21]. These observations may explain in part the correlation of ANXA4 with modulation of drug susceptibility in cancer cells.

This study demonstrates for the first time elevated ANXA4 protein expression in malignant mesothelioma cells that have less susceptibility to CDDP. *In vitro* evaluation of drug susceptibility against CDDP in malignant mesothelioma cells derived from cancer patients would be important in clinical conditions because doctors as well as patients wish to avoid treatment with inefficacious drugs. Consequently, the susceptibility of a given patient against CDDP could be confirmed by analyzing the expression level of ANXA4 in malignant mesothelioma patients at the time of diagnosis. Furthermore, if ANXA4 expression could be blocked specifically in malignant mesothelioma cells by nucleic acid drugs such as siRNA, this procedure would prove useful in clinical situations involving CDDP treatment. The present study may contribute to

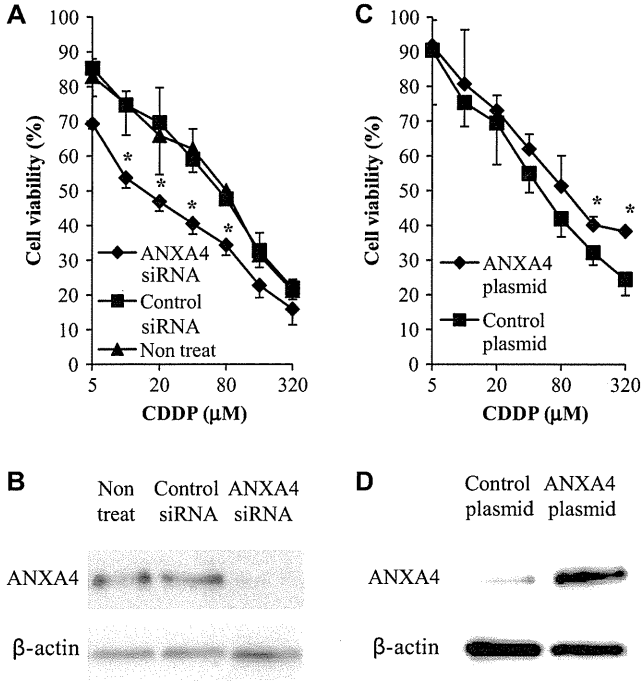

Fig. 4. The effect of ANXA4 gene knockdown and overexpression on CDDP susceptibility in malignant mesothelioma cells. Transfection of ANXA4 siRNA or plasmid into malignant mesothelioma cells confers resistance to CDDP. Cell survival after 24 h treatment of H28/ANXA4 siRNA or H2052/ANXA4 plasmid with different concentrations of CDDP (A and C). Expression of ANXA4 was analyzed by western blot analysis (B and D). Data are shown as means and standard deviations ($n = 4$). *$P < 0.05$ (Control siRNA or plasmid vs. ANXA4 siRNA or plasmid).

establishment of a new therapeutic strategy for malignant mesothelioma patients by suggesting a novel diagnostic and therapeutic target.

Acknowledgments

This study was supported in part by Grants-in-Aid for Scientific Research from the Ministry of Education, Culture, Sports, Science and Technology of Japan, and from the Japan Society for the Promotion of Science (JSPS). This study was also supported in part by Health Labor Sciences Research Grants from the Ministry of Health, Labor and Welfare of Japan and by Health Sciences Research Grants for Research on Publicly Essential Drugs and Medical Devices from the Japan Health Sciences Foundation.

References

[1] W.N. Rom, W.D. Travis, A.R. Brody, Cellular and molecular basis of the asbestos-related diseases, Am. Rev. Respir. Dis. 143 (1991) 408–422.
[2] N.H. Heintz, Y.M. Janssen-Heininger, B.T. Mossman, Asbestos, lung cancers, and mesotheliomas: from molecular approaches to targeting tumor survival pathways, Am. J. Respir. Cell Mol. Biol. 42 (2010) 133–139.
[3] Consensus Report: Asbestos, asbestosis, and cancer: the Helsinki criteria for diagnosis and attribution. Scand. J. Work Environ. Health 23 (1997) 311–316.
[4] T.D. Yan, L. Welch, D. Black, P.H. Sugarbaker, A systematic review on the efficacy of cytoreductive surgery combined with perioperative intraperitoneal chemotherapy for diffuse malignancy peritoneal mesothelioma, Ann. Oncol. 18 (2007) 827–834.
[5] E. Chailleux, D. Pioche, S. Chopra, G. Dabouis, P. Germaud, A.Y. De Lajartre, M. De Lajartre, Prognostic factors in diffuse malignant pleural mesothelioma: a study of 167 patients, Chest 93 (1988) 159–162.
[6] K.S. Sridhar, R. Doria, W.A. Raub Jr., R.J. Thurer, M. Saldana, New strategies are needed in diffuse malignant mesothelioma, Cancer 70 (1992) 2969–2979.
[7] M. Markman, D. Kelsen, Efficacy of cisplatin-based intraperitoneal chemotherapy as treatment of malignant peritoneal mesothelioma, J. Cancer Res. Clin. Oncol. 118 (1992) 547–550.
[8] G.H. Eltabbakh, M.S. Piver, R.E. Hempling, F.O. Recio, M.E. Intengen, Clinical picture, response to therapy, and survival of women with diffuse malignant peritoneal mesothelioma, J. Surg. Oncol. 70 (1999) 6–12.
[9] T. Berghmans, M. Paesmans, Y. Lalami, I. Louviaux, S. Luce, C. Mascaux, A.P. Meert, J.P. Sculier, Activity of chemotherapy and immunotherapy on malignant mesothelioma: a systematic review of the literature with meta-analysis, Lung. Cancer 38 (2002) 111–121.
[10] H.J. Lerner, D.A. Schoenfeld, A. Martin, G. Falkson, E. Borden, Malignant mesothelioma: The Eastern Cooperative Oncology Group (ECOG) experience, Cancer 52 (1983) 1981–1985.
[11] D.M. Mintzer, D. Kelsen, D. Frimmer, R. Heelan, R. Gralla, Phase II trial of high-dose cisplatin in patients with malignant mesothelioma, Cancer Treat Rep. 69 (1985) 711–712.
[12] B.L. Zidar, S. Green, H.I. Pierce, R.W. Roach, S.P. Balcerzak, L. Militello, A phase II evaluation of cisplatin in unresectable diffuse malignant mesothelioma: a Southwest Oncology Group Study, Invest New Drugs 6 (1988) 223–226.
[13] E.K. Han, S.K. Tahir, S.P. Cherian, N. Collins, S.C. Ng, Modulation of paclitaxel resistance by annexin IV in human cancer cell lines, Br. J. Cancer 83 (2000) 83–88.
[14] A. Kim, T. Enomoto, S. Serada, Y. Ueda, T. Takahashi, B. Ripley, T. Miyatake, M. Fujita, C.M. Lee, K. Morimoto, M. Fujimoto, T. Kimura, T. Naka, Enhanced expression of Annexin A4 in clear cell carcinoma of the ovary and its association with chemoresistance to carboplatin, Int. J. Cancer 125 (2009) 2316–2322.
[15] M.A. Kaetzel, P. Hazarika, J.R. Dedman, Differential tissue expression of three 35-kDa annexin calcium-dependent phospholipid-binding proteins, J. Biol. Chem. 264 (1989) 14463–14470.
[16] G. Zanotti, G. Malpeli, F. Gliubich, C. Folli, M. Stoppini, L. Olivi, A. Savoia, R. Berni, Structure of the trigonal crystal form of bovine annexin IV, Biochem. J. 329 (1998) 101–106.
[17] M.A. Kaetzel, Y.D. Mo, T.R. Mealy, B. Campos, W. Bergsma-Schutter, A. Brisson, J.R. Dedman, B.A. Seaton, Phosphorylation mutants elucidate the mechanism of annexin IV-mediated membrane aggregation, Biochemistry 40 (2001) 4192–4199.
[18] W.G. Hill, M.A. Kaetzel, B.K. Kishore, J.R. Dedman, M.L. Zeidel, Annexin A4 reduces water and proton permeability of model membranes but does not alter aquaporin 2-mediated water transport in isolated endosomes, J. Gen. Physiol. 121 (2003) 413–425.
[19] M.A. Kaetzel, H.C. Chan, W.P. Dubinsky, J.R. Dedman, D.J. Nelson, A role for annexin IV in epithelial cell function. Inhibition of calcium-activated chloride conductance, J. Biol. Chem. 269 (1994) 5297–5302.
[20] H. Sohma, C.E. Creutz, S. Gasa, H. Ohkawa, T. Akino, Y. Kuroki, Differential lipid specificities of the repeated domains of annexin IV, Biochim. Biophys. Acta 1546 (2001) 205–215.
[21] A. Piljic, C. Schultz, Annexin A4 self-association modulates general membrane protein mobility in living cells, Mol. Biol. Cell 17 (2006) 3318–3328.

Cytokine 61 (2013) 578–584

Contents lists available at SciVerse ScienceDirect

Cytokine

journal homepage: www.journals.elsevier.com/cytokine

Mutants of lymphotoxin-α with augmented cytotoxic activity *via* TNFR1 for use in cancer therapy

Tomohiro Morishige [a,1], Yasuo Yoshioka [b,c,*,1], Shogo Narimatsu [a], Shinji Ikemizu [d], Shin-ichi Tsunoda [c,e], Yasuo Tsutsumi [b,c,e], Yohei Mukai [a], Naoki Okada [a], Shinsaku Nakagawa [a,c,*]

[a] *Laboratory of Biotechnology and Therapeutics, Graduate School of Pharmaceutical Sciences, Osaka University, 1-6 Yamadaoka, Suita, Osaka 565-0871, Japan*
[b] *Laboratory of Toxicology and Safety Science, Graduate School of Pharmaceutical Sciences, Osaka University, 1-6 Yamadaoka, Suita, Osaka 565-0871, Japan*
[c] *The Center for Advanced Medical Engineering and Informatics, Osaka University, 1-6 Yamadaoka, Suita, Osaka 565-0871, Japan*
[d] *Graduate School of Pharmaceutical Sciences, Kumamoto University, 5-1 Oe-honmachi, Kumamoto 862-0973, Japan*
[e] *Laboratory of Biopharmaceutical Research, National Institute of Biomedical Innovation, 7-6-8 Saito-Asagi, Ibaraki, Osaka 567-0085, Japan*

ARTICLE INFO

Article history:
Received 6 July 2012
Received in revised form 29 September 2012
Accepted 6 November 2012
Available online 11 December 2012

Keywords:
Affinity
Apoptosis
Bioactivity
Cytokine
Cytotoxicity

ABSTRACT

The cytokine lymphotoxin-α (LTα) is a promising candidate for use in cancer therapy. However, the instability of LTα *in vivo* and the insufficient levels of tumor necrosis factor receptor 1 (TNFR1)-mediated bioactivity of LTα limit its therapeutic potential. Here, we created LTα mutants with increased TNFR1-mediated bioactivity by using a phage display technique. We constructed a phage library displaying lysine-deficient structural variants of LTα with randomized amino acid residues. After affinity panning, we screened three clones of lysine-deficient LTα mutant, and identified a LTα mutant with TNFR1-mediated bioactivity that was 32 times that of the wild-type LTα (wtLTα). When compared with wtLTα, the selected clone showed augmented affinity to TNFR1 due to slow dissociation rather than rapid association. In contrast, the mutant showed only 4 times the TNFR2-mediated activity of wtLTα. In addition, the LTα mutant strongly and rapidly activated caspases that induce TNFR1-mediated cell death, whereas the mutant and wtLTα activated nuclear factor-kappa B to a similar extent. Our data suggest that the kinetics of LTα binding to TNFR1 play an important role in signal transduction patterns, and a TNFR1-selective LTα mutant with augmented bioactivity would be a superior candidate for cancer therapy.

1. Introduction

Lymphotoxin-alpha (LTα) is a tumor necrosis factor (TNF) superfamily cytokine with tumor-cell-specific cytotoxic activity and immune-activating activity. LTα induces the expression of chemokines and adhesion molecules in endothelial cells, and plays a key role in lymph node neogenesis [1–3]. Schrama et al. [4,5] showed that systemic administration of LTα to a tumor-bearing mouse leads to the construction of ectopic lymphoid tissue within the tumor and the strong induction of tumor immunity in that lymphoid tissue, suggesting that the underlying mechanism of this cytokine's anti-tumor activity may be effective. Therefore, LTα has long been considered to be a promising candidate for an anti-cancer agent. However, the clinical use of LTα has been limited because of the protein's *in vivo* instability and proinflammatory side effects.

One of the most common ways to improve the therapeutic effects of proteins is to conjugate them with polyethylene glycol (PEG) in a process called PEGylation, or to conjugate them with other water-soluble polymers [6]. Because of the steric hindrance caused by the PEG molecule, PEGylation can prolong the plasma half-life of molecules and alter the tissue distribution of the conjugates compared with those of the native form. PEGylation of proteins is mostly nonspecific because it targets all of the lysine residues in the protein, some of which may be in or near an active site. As a result, PEGylation significantly reduces the specific

Abbreviations: E. coli, Escherichia coli; ELISA, enzyme-linked immunosorbent assay; FADD, Fas-associated protein with death domain; FBS, fetal bovine serum; HVEM, herpes virus entry mediator; IFNγ, interferon γ; LTα, lymphotoxin-alpha; NFκB, nuclear factor-kappa B; PEG, polyethylene glycol; pI, isoelectric points; SDS–PAGE, sodium dodecyl sulfate–polyacrylamidegel electrophoresis; SPR, surface plasmon resonance; TNF, tumor necrosis factor; TNFR1, TNF receptor 1; TRADD, TNF receptor-associated death domain; TRAF, TNF receptor-associated factor; wtLTα, wild-type LTα.

* Corresponding authors. Addresses: Laboratory of Toxicology and Safety Science, Graduate School of Pharmaceutical Sciences, Osaka University, 1-6 Yamadaoka, Suita, Osaka 565-0871, Japan. Tel./fax: +81 6 6879 8233 (Y. Yoshioka), Laboratory of Biotechnology and Therapeutics, Graduate School of Pharmaceutical Sciences, Osaka University, 1-6 Yamadaoka, Suita, Osaka 565-0871, Japan. Tel.: +81 6 6879 8175; fax: +81 6 6879 8179 (S. Nakagawa).

E-mail addresses: yasuo@phs.osaka-u.ac.jp (Y. Yoshiokab), nakagawa@phs.osaka-u.ac.jp (S. Nakagawa).

[1] These authors contributed equally to the work.

1043-4666/$ - see front matter © 2012 Elsevier Ltd. All rights reserved.
http://dx.doi.org/10.1016/j.cyto.2012.11.005